Latch, Spring and Release: The Efficiency of Power-Amplified Jumping

Marc Suñé,[1,*] Lucas Selva,[1] Cristóbal Arratia,[2] John Wettlaufer,[2,3,†] and Dominic Vella[1,‡]

[1] *Mathematical Institute, University of Oxford, Oxford OX2 6GG, United Kingdom*
[2] *Nordita, Royal Institute of Technology and Stockholm University, Hannes Alfvéns väg 12, SE-106 91 Stockholm, Sweden*
[3] *Yale University, New Haven, Connecticut 06520, USA and Nordita, Royal Institute of Technology and Stockholm University, Hannes Alfvéns väg 12, SE-106 91 Stockholm, Sweden*

(Dated: October 20, 2025)

Many small animals, particularly insects, use power-amplification to generate rapid motions such as jumping, which would otherwise not be possible with the standard power density of muscle. A common framework for understanding this power amplification is Latch-Mediated, Spring Actuated (or LaMSA) jumping, in which a spring is slowly compressed, latched in its compressed state and the latch released to allow jumping. Motivated by the jumps of certain insect larvae, we consider a variant of this in which the latching occurs externally via adhesion to a substrate that is quickly released for jumping. We show that the rate at which this adhesion is lost is crucial in determining the efficiency of jumping and, indeed, whether jumping occurs at all. As well as showing how release rate should be chosen to facilitate optimal jumping, our analysis suggests that it is possible to control jumps even once the latch has been set.

Power amplification is an important strategy for generating fast motion in both the engineering and natural sciences: an archer stores energy slowly in the string of a bow that allows the arrow to fly faster when released than would have been the case if it had simply been thrown [1]. Similarly, plants such as the Venus flytrap [2] and insects such as the family of 'click' beetles [3] are able to generate rapid motions or jumps by storing energy slowly in an effective spring that is released quickly when required.

A key ingredient for exploiting this power amplification is being able to control the release. An internal 'latch' is the common way of understanding this with a latching mechanism being explicitly identified in the click beetles, for example [3]. The integration of a motor, spring and latch to generate rapid motion is a generic strategy that has been categorized under the umbrella of 'Latch-Mediated, Spring Actuated' (or LaMSA) mechanisms [4]. The spring is typically loaded at low power by the motor and then latched, ready to be released when desired (for example, when an insect needs to avoid a predator). While this mechanism is very effective at releasing energy quickly when required, as typically presented, it suggests very little control over the way in which the resulting motion occurs — once the spring is loaded, how can one control features of the motion such as the jump height (for a click beetle) or the speed of the arrow (for an archer)?

Latch mechanisms are usually embodied in the elastic body itself as for the click beetles [3], but also in artificial jumping systems [5, 6]. However, in other cases another body (most often a substrate) serves as an anchor and the effective latch is the connection between the jumper and substrate. This unusual 'external latch' behavior is exhibited by some larval beetles [7]. It is understood that the larva attaches its legs to the substrate and then arches its body dorsally by muscle contraction. Because of the attachment to the substrate, the arching of the larva's back does not significantly change the shape but effectively stores elastic energy in the elastic components of its body (the spring) while its legs grip the substrate (thereby forming the latch). When the legs begin to lose contact with the substrate, the constraint imposed by the latch is released and the body is able to return to its (now curved) natural state. In the process, the stored elastic energy is transferred to kinetic energy of jumping. The combination of relaxation to a curved shape and jumping is shown in fig. 1a.

To better understand this jumping mechanism, we consider confining a naturally curved elastic strip by poking it down at its center (mimicking the legs' grip on the substrate) and then releasing it. Figure 1b shows a superposition of the states that the arch goes through when the confining force is removed relatively slowly — the strip goes from being approximately flat to being naturally curved, but does not appear to lose contact with the substrate. However, if the confining force is removed more quickly — for example by hanging a weight below the arch via a thread that can readily be cut (as in fig. 1c) — then the strip is observed to jump from the substrate. Clearly, the strip stores elastic potential energy when it is indented that is then converted to kinetic energy. More surprisingly perhaps, the efficiency of this conversion depends on how quickly the indenting force is released. This raises the question of how the speed of release changes the efficiency of the conversion from elastic potential energy to kinetic energy of jumping.

The jumping larvae studied by Bertone *et al.* [7] exhibit a large scatter in the efficiency of this mechanism — the coefficient of variation of the kinetic energy at take off is

* marc.sunesimon@maths.ox.ac.uk
† john.wettlaufer@yale.edu
‡ dominic.vella@maths.ox.ac.uk

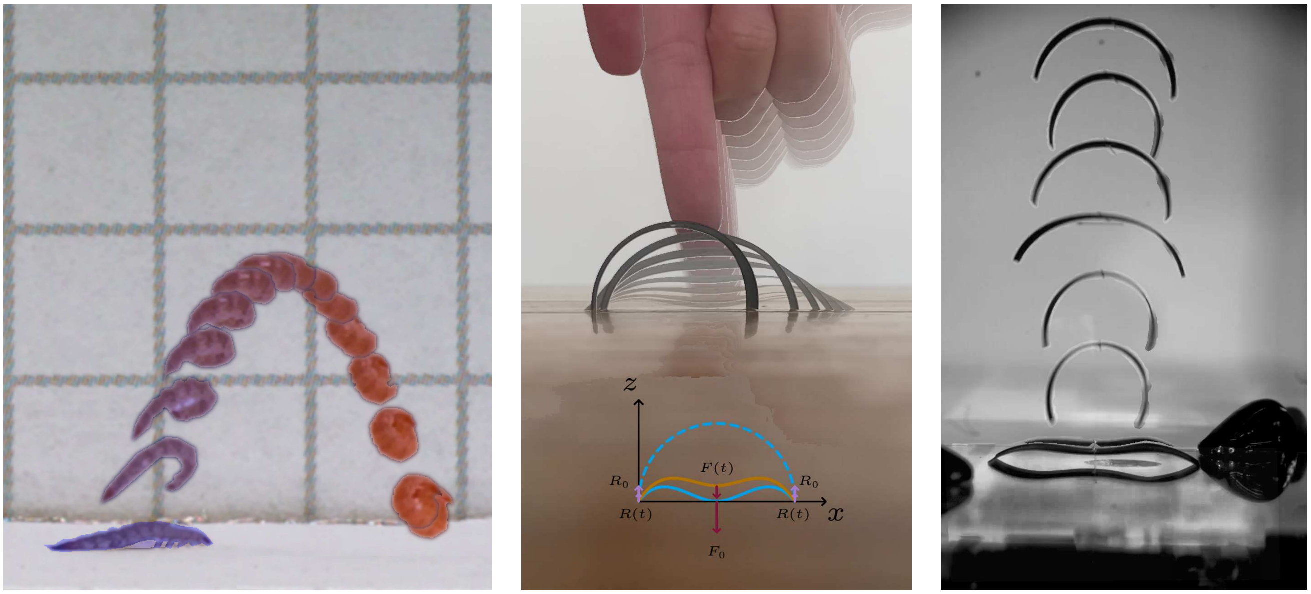

(a) (b) (c)

FIG. 1. Release rate control of externally-latched jumping. (a) Jumping behavior in larval beetles (*Laemophloeus biguttatus*). Adapted from Bertone *et al.* [7] (equally spaced frames show instants between $t = 0, 100$ ms after the initation of jumping.) (b-c) A curved elastic strip is initially indented at its center by a pressing finger (b) and a hanging weight (c). A low release rate does not result in jumping ((b), equally timed frames between up to 867 ms after first motion), while quick release does ((c) with equally timed frames up to 64 ms after first motion). Unlatching times in the time composite images (a-c) are $t_u = (5.5, 683, 1)$ ms. Inset in panel (b): Schematic representation of the shell in the xz-plane at three different configurations; in absence of external forces (other than its own weight) in dashed blue, when it is loaded at the center (in solid blue), and when the loading is partially released (orange).

about 25% for jumps of the same individual.

Given the role of release rate in the biomimetic example of a curved strip on a flat substrate, it is natural to examine the role of release rate in externally latched jumping as a means of controlling the jump characteristics even once the latch has been set. The cleanness of the mechanism of jumping in these examples allows us to build a simple mathematical model of latch-spring-actuated movement that includes normal substrate-system interactions, but neglects friction.

We consider a two-dimensional model of a naturally curved, linearly elastic and inextensible cylindrical shell that lies on the xz-plane and both ends are at $z = 0$ (see the schematic of the shell in navy blue in the lower inset in fig. 1b). The shell is in contact with a flat, rigid substrate perpendicular to the gravitational field (with acceleration g). We shall assume that contact only occurs at these two ends, simplifying the analysis considerably. The natural curvature of the shell is κ_0, and it has width b, volumetric mass density ρ, Young's modulus E, thickness h and length ℓ, with $h \ll \ell$.

Initially, an indenting force per unit width $f(t = 0) = f_0$ is applied at the center of the shell that confines it to lie almost parallel to a planar substrate (the green curve in the schematic of the shell in fig. 1b). This force serves as the motor (increasing and storing elastic energy within the deformed shell for $t < 0$). However, once the indenting force reaches $z = 0$, f plays the role of the latch, keeping the deformed shell confined — the shell is in equilibrium due to the reaction force of the substrate on the edges. For time $t > 0$ the indenting force is gradually released (the teal blue curve in the schematic of the shell in fig. 1b). We assume a simple model for latch dynamics with characteristic unlatching time t_u,

$$f(t) = f_0 \exp(-t/t_u). \tag{1}$$

In the following we non-dimensionalize lengths by ℓ, heights by $\ell^2|\kappa_0|$, masses by $\rho h \ell^2$, times by $(\rho h \ell^4/EI)^{1/2}$ (here $I = h^3/12$ is the moment of inertia of the shell per unit width), horizontal forces (per unit width) by EI/ℓ^2 and vertical forces (per unit width) by $EI|\kappa_0|/\ell$. We use upper case letters to denote dimensionless versions of the corresponding dimensional quantity, e.g. $X = x/\ell$, $Z = z/(|\kappa_0|\ell^2)$. In the limit of small, planar deflections of a slender shell, the dimensionless vertical coordinates of the shell, $Z(X, T)$, a time T after the gradual release of the force is initiated and before launching are given by the dimensionless dynamic beam equation [8];

$$\frac{\partial^4 Z}{\partial X^4} + \frac{\partial^2 Z}{\partial T^2} + H\frac{\partial Z}{\partial T} + 1/\beta = 0. \tag{2}$$

Here we neglect the tension within the shell, and hence the role of friction with the substrate; this is justified within the small angle approximation where the work done against friction is negligible because of the small horizontal distance moved by the contact points [9].

Two dimensionless groups defined by

$$\beta = \frac{EI|\kappa_0|}{\rho g h \ell^2} \quad \text{and} \quad H = \frac{2\eta\ell^2}{(EI\rho h)^{1/2}}, \tag{3}$$

are introduced. These measure the relative importance of bending forces to the gravitational force and the strength of damping relative to bending forces, respectively. Here η is the translational drag coefficient of the shell, and we use slender-body theory to model viscous forces on the shell [10]. In the experiments of fig. 1c, the typical value of β is approximately 10, while we estimate it for the larvae of fig. 1a to be $\beta \approx 1$; we must therefore account for gravity in what follows. Similarly, the limit of no damping, $H = 0$, is well defined but the decay of oscillations in our experiments suggests that $H \approx 2$.

The applied force $F(T)$ enters via a point loading condition at $X = 1/2$ — we assume that there is a discontinuity in the shear force there (or, equivalently, a Dirac delta-function external pressure there). We therefore have that

$$\left[\frac{\partial^3 Z}{\partial X^3}\right]_{X=1/2^-}^{X=1/2^+} = F_0 \exp(-T/\tau), \tag{4}$$

where τ is the scaled t_u and F_0 is the dimensionless f_0 (scaled by the characteristic vertical force per unit width).

The small-slope approximation simplifies the analytic treatment of the problem because, while the shell remains in contact with the substrate, the boundary conditions are fixed at $X = 0, 1$: $Z(0,T) = Z(1,T) = 0$ and $\partial^2 Z/\partial X^2\big|_{X=0,1} = \kappa_0/|\kappa_0|$. It also avoids energy being dissipated by friction with the substrate (since the edges do not move laterally, there is no work done).

We take as the initial condition that the indentation force is precisely that required to make the center touch the substrate, i.e. $Z(X, T=0) = Z_0(X)$ where $Z_0(X)$ is the solution to the linearized equilibrium problem

$$\frac{\mathrm{d}^4 Z_0}{\mathrm{d}X^4} + \frac{1}{\beta} = 0, \tag{5}$$

with analogous boundary conditions at $X = 0, 1$ and fixed height at $X = 1/2$, $Z_0(X = 1/2) = 0$. (The combination of these conditions yield a unique solution to eq. (5) in the form of a fourth order polynomial that is given in the supplementary information.) The value of F_0 in (4) is determined from the resulting discontinuity in the shear force. Finally, the shell is assumed to start from rest, so that $\partial Z/\partial T(X, T=0) = 0$.

The dynamic beam equation (2) with the boundary, initial and continuity conditions discussed above can be solved analytically by letting

$$Z(X,T) = \zeta(X,T) - w(X) - \exp(-T/\tau)\, y(X), \tag{6}$$

where $\zeta(X,T)$ is the separable solution of the homogeneous problem (which depends on the frequencies of natural oscillations $\omega_n = \frac{H}{2}\left(\frac{4n^4\pi^4}{H^2} - 1\right)^{1/2}$ in underdamped conditions $H < 2n^2\pi^2$), $w(X)$ is a particular solution that absorbs the inhomogeneous parts arising from the natural curvature and $y(X)$ is a particular solution that absorbs the discontinuity imposed by (4). Details of the functional forms for $\zeta(X,T)$, $w(X)$ and $y(X)$ are given in the supplementary information.

Both the jumping of the larvae and our tabletop experiments reveal a broad range of jumping behavior from failed attempts to leave the ground to effective (and impressive) jumps; there is clearly a large variability in the efficiency of this mechanism. We rationalize this behavior in terms of the three dimensionless parameters in the model β, τ and H. We begin by noting that the scaled reaction force of the ground on the edge of the shell, R, can only be positive — if this reaction force becomes negative then the shell has lost contact with the ground, and the shell has jumped. Noting that R may be calculated from the solution $Z(X,T)$, eq. (6) as

$$R(T) = \left.\frac{\partial^3 Z}{\partial X^3}\right|_{X=0}. \tag{7}$$

We then build the phase space of the failure/success in jumping from the analytical solution of the linearized model, eq. (6), finding the smallest positive root of $R(T) = 0$ numerically using the *Chebfun* package [11] in *Matlab*. The results in fig. 2a show that the shell jumps for larger β (light, stiff shell), smaller τ (quick release) and H (small dissipation), but also that it fails to jump for smaller β (heavy shell), larger τ (slow release) and H (large dissipation).

In undamped conditions ($H = 0$), for light, stiff shells (i.e. away from the small β limit), the phase boundary in the (β, τ) plane is linear. An asymptotic approximation of the analytical solution eq. (6) — obtained by truncating at the fundamental mode ($n = 1$) and considering the limit of large τ and large T/τ — allows us to calculate an approximation of $R(T)$ and, upon imposing the condition that the minima in this approximation equal to zero, we find an estimate of the phase boundary $\tau_{\text{boundary}}(\beta) \sim \frac{24}{\pi^3}\beta$ (a detailed derivation is provided in the supplementary information) that shows good agreement with numerical results for $\beta > 1$ (see fig. 2b). This boundary becomes noticeably sublinear as the dissipation H increases: jumping requires a quicker unlatching for more strongly damped systems. Moreover, regardless of the damping H, a strong nonlinear deviation of the phase boundary also occurs for small β (fig. 2b). The phase boundary crosses the abscissa at $\beta \sim \beta_{\text{crit}}$, where $\beta_{\text{crit}} = \frac{1}{2}\frac{\left(\frac{5}{2}+\pi\right)}{12+\pi}$ is an estimation (by asymptotic arguments, see the supplementary information) of the minimal β for jumping. This minimum is motivated by the fact that a sufficiently heavy shell will bend due to its own weight and hence naturally satisfy the condition $Z_0(X = 1/2) = 0$ at zero external force.

The phase space in fig. 2 quantifies the intuition that a faster unlatching mechanism facilitates jumping. We therefore expect that a jumping mechanism should be

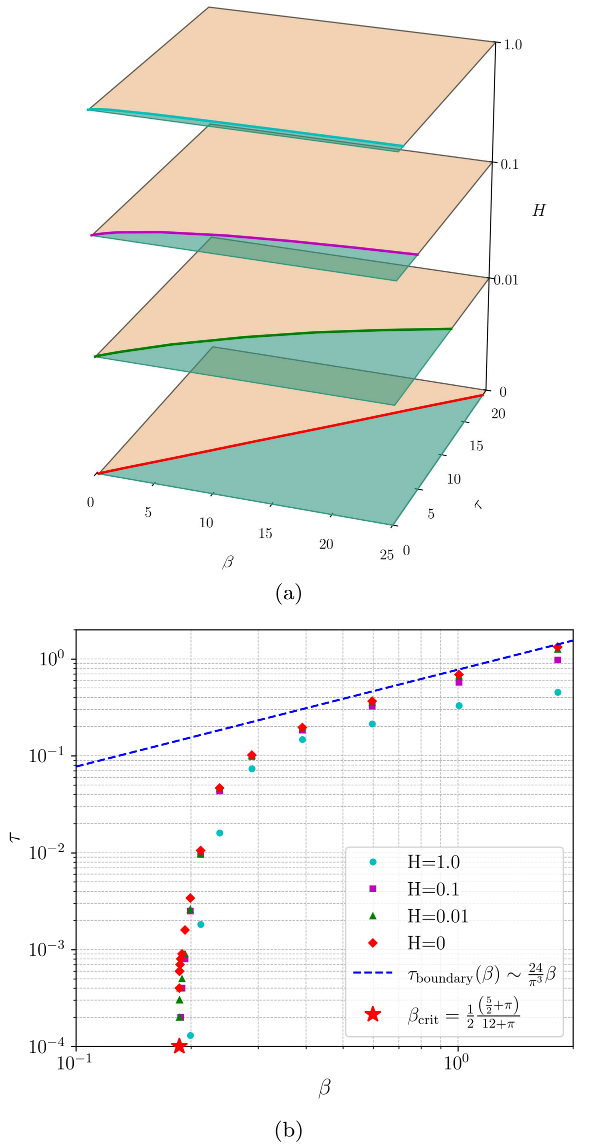

FIG. 2. (a) Phase diagram of the jumping behavior of a curved shell on a flat surface at different values of the damping H. The jumping behavior of the shell is characterized by the triad (β, τ, H): there is a jumping phase (in green) and a non-jumping phase (in orange). (b) Phase boundaries at different values of parameter H and small (β, τ). The colour scheme of the boundaries in (a) is the same as in (b).

designed to ensure the fastest possible unlatching. However, the larvae studied by Bertone *et al.* [7] seem to contradict this basic principle as they grip the substrate with all their legs, which presumably results in a slower latch release. To understand this apparent paradox we examine the maximum dimensional latch force F_0 — i.e. the attaching force between the larva's legs and the substrate — and the stored energy (bending + gravitational). The results of this calculation show (fig. 3) that the magnitude of the latch force increases approximately linearly as the curvature increases — even when geometrical nonlinearities are accounted for. However, the stored energy shows a superlinear increase with curvature (see SI fig. S6). Detailed experiments on other insect larvae [12] show that the legs are typically able to supply a maximum adhesive force of $0.3 - 0.6$ mN. Assuming that each pair of legs is able to produce a similar force, and noting that they are located nearby one another (and hence can be assumed to be approximately a point force), using multiple legs to anchor on the surface should increase the maximum natural curvature obtained before release by a factor of 3 and the energy stored by a factor of 9. We therefore estimate the maximum latch force that can be generated by *Laemophloeus biguttatus* should be around 0.2 mN (approximating its body by a rod of radius ~ 0.6 mm). In our model, this corresponds to a maximum natural curvature $\kappa_0^{\max}$, but to determine the corresponding dimensional value requires an estimate of the effective Young's modulus of the larva. We obtain such an estimate by using the time scale of the return to the naturally curved state once the jump has been initiated, and comparing this to theoretical work on the curling of a ribbon by Callan-Jones *et al.* [13]; this leads us to estimate $E_{\mathrm{eff}} \sim 10$ kPa, and corresponds to $|\kappa_0^{\max}| = 1.69\ \mathrm{mm}^{-1}$ (see SI). Figure 3 shows that these estimates are consistent. Finally, we hypothesize that once the maximum force is exceeded at one point and the adhesion between leg and substrate fails, then the remaining legs are successively detached.

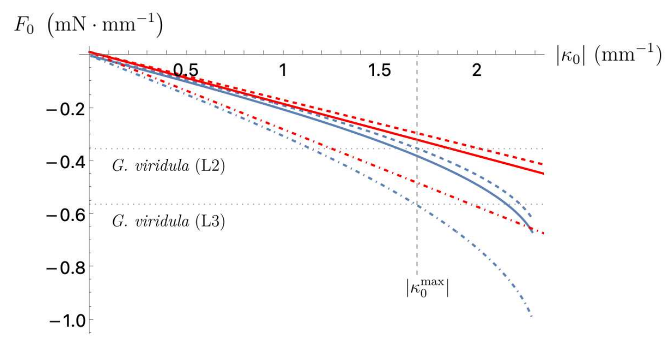

FIG. 3. Latch force required for an indented, naturally curved, shell with dimensions from *Laemophloeus biguttatus* [7]. Latch force as a function of the shell's curvature given by the linearized theory (in red) and the non-linear model (in blue). Line styles denote different Young's modulus: $E \sim 10$ kPa (estimated value from the time scale of curling of an elastic object [13], solid lines); $E \sim 9.25$ kPa (estimated value from the attachment force of 2nd instar of *G. viridula* [12], dashed lines); $E \sim 14.9$ kPa (estimated value from the attachment force of 3rd instar of *G. viridula* [12], dot–dashed lines). (Here 'instar' refers to different developmental stages of insects, between moulting of the exoskeleton.)

A key parameter of importance in the space of LaMSA mechanisms is the efficiency of the release mechanism: what percentage of the elastic energy that is initially stored is realized as translational kinetic energy upon release? Yang and Kim [5] measured this for elastic jumping hoops and found that it is a universal quan-

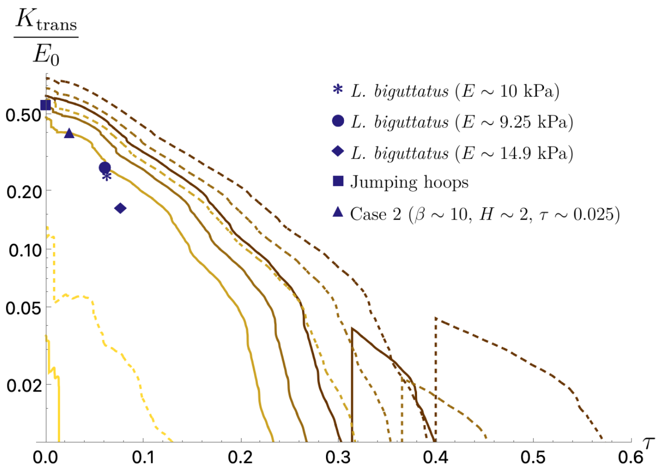

FIG. 4. Energy efficiency of jumping of a curved shell given by the ratio of translational kinetic energy at $T = T_{\rm off}$ to stored energy at $T = 0$ as a function of the latch lifting time scale. Theoretical predictions from linearized theory are depicted in solid lines. Scaled values of the efficiency for *L. biguttatus* [7], jumping hoops [5], and our experiments of a curved strip are also included as symbols. Solid lines for $\beta = 1$ and dashed lines for $\beta = 10$. Colors range from dark brown (small H) to yellow (large H) for $H = 0.1, 1, 2, 10$,

tity, around 57%, independent of the material properties of their system. While it is difficult to ascribe a precise value of τ to their experimental technique, it is very small, and agrees well with the predicted efficiency when $\tau \approx 0$. Here, we are able to readily calculate the efficiency of jumping, defined as

$$\mathcal{E} = \frac{K_{\rm trans}}{E_0} \times 100\% \tag{8}$$

directly from the solution in (6). Our results for $\mathcal{E}(\tau)$ are shown for a variety of values of β and H in fig. 4. As might have been expected, these show that the efficiency of jumping decreases with τ, though it is somewhat surprising that our results suggest that this decay appears to be exponential. Moreover, there appear to be certain *pessimal* values of τ where the efficiency drops even more dramatically (we estimate these pessimal values in the SI using asymptotic methods). We attribute this to a destructive interference between the imposed decay of $F(t)$ and the natural relaxation time of the shell, which is consistent with the re-entrant efficiency observed for lighter, stiffer shells.

The sensitive dependence of the efficiency of jumping on the release time scale τ suggests a rationalization for the wide variability in the efficiency of jumps that were reported by Bertone *et al.* [7]: even an apparently small change in the latch release time τ can lead to a large decrease in the efficiency of jumping. This complements previous studies, which have focussed on the role of latch geometry and release velocity in control of energy release with internal latches [14, 15].

We have developed a dynamical theory that describes the observed efficiency of the jumps of insect larvae, as well as providing a mechanism for the wide distribution of observed jump efficiencies: an exponential decay means that small changes in τ lead to significantly less efficient jumps. While this may pose a substantial challenge to insect larvae, it also focuses the design criteria for controlling jumps in robots [6], for example. To make this a reality, however, may require generalizing this work to scenarios where the contact set is more complicated than that considered here — for example, in insect-inspired jumping robots, the contact region grows during the early stages of jumping, before ultimately decreasing [6].

ACKNOWLEDGMENTS

This work was partially supported by the UK Engineering and Physical Sciences Research Council via Grant No. EP/W016249/1 and Grant No. EP/Y027949/1 (M.S. and D.V.), and by the Swedish Research Council under Grant No. 638-2013-9243 (M.S. and J.W.). For the purpose of Open Access, the authors will apply a CC BY public copyright license to any Author Accepted Manuscript version arising from this submission.

[1] A. Galantis and R. C. Woledge, The theoretical limits to the power output of a muscle–tendon complex with inertial and gravitational loads, Proc. R. Soc. Lond. B **270**, 1493 (2003).

[2] Y. Forterre, J. M. Skotheim, J. Dumais, and L. Mahadevan, How the Venus flytrap snaps, Nature **433**, 421 (2005).

[3] O. Bolmin, J. J. Socha, M. Alleyne, A. C. Dunn, K. Fezzaa, and A. A. Wissa, Nonlinear elasticity and damping govern ultrafast dynamics in click beetles, Proc. Natl Acad. Sci. USA **118**, e2014569118 (2021).

[4] M. Ilton, M. S. Bhamla, X. Ma, S. M. Cox, L. L. Fitchett, Y. Kim, J.-s. Koh, D. Krishnamurthy, C.-Y. Kuo, F. Z. Temel, A. J. Crosby, M. Prakash, G. P. Sutton, R. J. Wood, E. Azizi, S. Bergbreiter, and S. N. Patek, The principles of cascading power limits in small, fast biological and engineered systems, Science **360**, eaao1082 (2018).

[5] E. Yang and H.-Y. Kim, Jumping hoops, Am. J. Phys. **80**, 19 (2012).

[6] Y. Wang, Q. Wang, M. Liu, Y. Qin, L. Cheng, O. Bolmin, M. Alleyne, A. Wissa, R. H. Baughman, D. Vella, and S. Tawfick, Insect-scale jumping robots enabled by a dynamic buckling cascade, Proc. Natl Acad. Sci. USA **120**, e2210651120 (2023).

[7] M. A. Bertone, J. C. Gibson, A. E. Seago, T. Yoshida,

and A. A. Smith, A novel power-amplified jumping behavior in larval beetles (coleoptera: Laemophloeidae), PLOS One **17**, e0256509 (2022).

[8] P. Howell, G. Kozyreff, and J. Ockendon, *Applied Solid Mechanics*, Cambridge Texts in Applied Mathematics (Cambridge University Press, 2008).

[9] K. Yoshida and H. Wada, Mechanics of a snap fit, Phys. Rev. Lett. **125**, 194301 (2020).

[10] R. G. Cox, The motion of long slender bodies in a viscous fluid part 1. general theory, J. Fluid Mech. **44**, 791–810 (1970).

[11] T. A. Driscoll, N. Hale, and L. N. Trefethen, eds., *Chebfun Guide* (Pafnuty Publications, 2014).

[12] D. B. Zurek, S. N. Gorb, and D. Voigt, Locomotion and attachment of leaf beetle larvae *Gastrophysa viridula* (coleoptera, chrysomelidae), Interf. Focus **5**, 20140055 (2015).

[13] A. C. Callan-Jones, P. T. Brun, and B. Audoly, Self-similar curling of a naturally curved elastica, Phys. Rev. Lett. **108**, 174302 (2012).

[14] S. Divi, X. Ma, M. Ilton, R. St. Pierre, B. Eslami, S. N. Patek, and S. Bergbreiter, Latch-based control of energy output in spring actuated systems, J. R. Soc. Interface **17**, 20200070 (2020).

[15] S. Divi, R. St. Pierre, H. M. Foong, and S. Bergbreiter, Controlling jumps through latches in small jumping robots, Bioinspir. Biomim. **18**, 066003 (2023).

Supplementary Information for "Latch, Spring and Release: The Efficiency of Power-Amplified Jumping"

Marc Suñé, Lucas Selva, Cristóbal Arratia, John Wettlaufer, and Dominic Vella

In this Supplementary Information we present further details of the two-dimensional model of the cylindrical shell (§ S1), its resolution both analytically and numerically (§ S2), and the analysis of the jumping behavior (§ S3). We also briefly describe the experiments with a naturally curved strip (§ S3 E).

S1. MODEL: CYLINDRICAL CAP AND LATCH MECHANISM

We consider the planar elastic unshearable deformations of a naturally curved, linearly elastic, homogeneous, isotropic and inextensible cylindrical cap. The cylindrical cap forms a shell that lies in the xz-plane with both ends at $z = 0$, as shown in fig. S1. The plane $z = 0$ represents a flat, rigid substrate and is perpendicular to the gravitational field (with acceleration g). We shall assume that contact only occurs at the two ends of the cylindrical cap.

The shape of the shell is parametrized by the arc length s measured along the centerline from the left end, $s \in [0, \ell]$, with tangent angle θ — the angle the tangent vector makes with the horizontal axis. In the absence of any external forces, the shell has constant curvature κ_0 so that its undeformed shape, $\theta = \theta_0(s)$, satisfies

$$\frac{\mathrm{d}\theta_0(s)}{\mathrm{d}s} = \kappa_0. \tag{S1}$$

The centerline of the shell, $\mathbf{r}(s) = [x(s), z(s)]$, is given by

$$\frac{\partial \mathbf{r}}{\partial s} = \cos\theta\, \mathbf{e}_x + \sin\theta\, \mathbf{e}_z, \tag{S2}$$

where $\mathbf{e}_x$ and $\mathbf{e}_z$ are unit vectors respectively in the x and z directions.

The shell has volumetric mass density ρ, Young's modulus E, moment of inertia (per unit width) $I = \frac{h^3}{12}$, thickness h, width b, and length ℓ, with $h \ll \ell$.

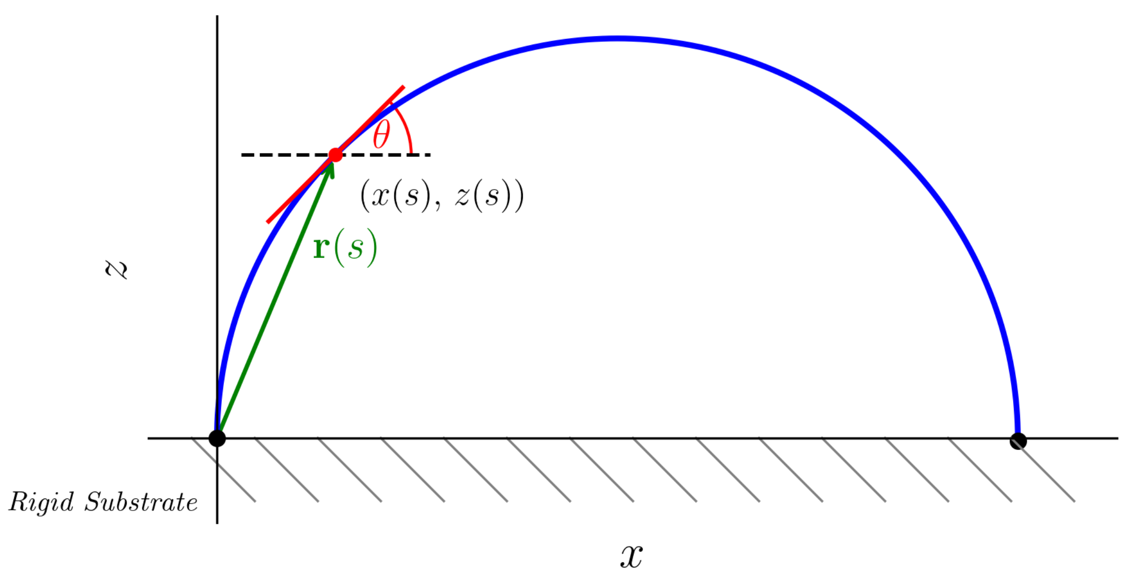

FIG. S1. Schematic representation of the cylindrical cap in the xz-plane.

A. Dynamic beam equation

1. Variational principle

The equations describing the evolution of the shell's shape can be derived from a variational principle [1]. We consider the system's generalized coordinates $\mathbf{q} = (x, z, \theta)$. We seek to minimize the action $\mathcal{S}[\mathbf{q}] = \int_{t_1}^{t_2} \mathrm{d}t\, \mathcal{L}\Big(\mathbf{q}, \dot{\mathbf{q}}(t), t\Big)$, with t denoting time, dots denoting differentiation with respect to t, and $\mathcal{L}\Big(\mathbf{q}, \dot{\mathbf{q}}(t), t\Big)$ denoting the Lagrangian of the system:

$$\mathcal{L}\Big(\mathbf{q}, \dot{\mathbf{q}}(t), t\Big) = \mathcal{T} - \mathcal{V} - \lambda_x(s,t)\left(\frac{\partial x}{\partial s} - \cos\theta\right) - \lambda_z(s,t)\left(\frac{\partial z}{\partial s} - \sin\theta\right) - L\,\lambda_g(t)\int_0^L \mathrm{d}s\,\sin\theta. \tag{S3}$$

The system has kinetic energy $\mathcal{T}$, considering translational and rotational contributions,

$$\mathcal{T} = \frac{1}{2}\int\int\int \mathrm{d}V\,\rho\left(\dot{x}^2 + \dot{z}^2 + z^2\dot{\theta}^2\right) = \frac{1}{2}b\rho\int_0^\ell \mathrm{d}s\left[h\left(\dot{x}^2 + \dot{z}^2\right) + \frac{h^3}{12}\dot{\theta}\right]; \tag{S4}$$

and potential energy $\mathcal{V}$, which includes gravitational and bending contributions,

$$\mathcal{V} = \int_0^\ell \mathrm{d}s\left[\frac{1}{2}bEI\left(\frac{\mathrm{d}\theta}{\mathrm{d}s} - \kappa_0\right)^2 + \rho g b h\, z(s)\right]. \tag{S5}$$

We enforce the inextensibility of the shell (i.e. the parameter s is the true arc length) and (local) geometric consistency by using Lagrange multipliers $\lambda_{x,z}(s,t)$. $\lambda_g(t)$ represents the Lagrange multiplier used to enforce the global constraint that both end-points of the shell must have the same vertical position.

Using the Euler–Lagrange equations with this variational principle we obtain the balance of angular momentum:

$$-\rho I\frac{\partial^2\theta}{\partial t^2} + EI\frac{\partial^2\theta}{\partial s^2} - \rho g h(\ell - s)\,\cos\theta - \lambda_x(s,t)\,\sin\theta + \lambda_z(s,t)\,\cos\theta - \lambda_g(t)\,\cos\theta = 0; \tag{S6}$$

and the balance of forces in each direction:

$$\rho h\frac{\partial^2 x}{\partial t^2} - \frac{\partial\lambda_x(s,t)}{\partial s} = 0, \quad \text{and} \tag{S7}$$

$$\rho h\frac{\partial^2 z}{\partial t^2} - \frac{\partial\lambda_z(s,t)}{\partial s} = 0. \tag{S8}$$

Considering freely rotating and freely (horizontally) moving ends — recall that we assumed fixed vertical positions for the ends — the boundary conditions are:

$$\left.\frac{\partial\theta(s,t)}{\partial s}\right|_{s=0,\ell} = \kappa_0, \quad \text{and} \quad \lambda_x(s,t)\Big|_{s=0,\ell} = 0. \tag{S9}$$

These boundary conditions implicitly assume the neglect of friction between the shell's endpoints and the ground, we will discuss this assumption further later.

2. Dissipation

To model the jumping behavior of slender elastic shells we introduce dissipation into eqs. (S6,S7,S8). The shell is confined in the xz-plane and hence has three degrees of freedom: rotations about an axis perpendicular to the plane, and translations along the x, z directions. By virtue of the small-slope approximation — that we will introduce later — these translations are approximately the axial and horizontal translations of a slender body. Considering the resistance of the surrounding fluid on the moving shell, slender-body theory [2] predicts that the horizontal drag coefficient (we omit here its expression in terms of the geometrical parameters of the shell) is approximately twice the axial drag, η. Thus, viscous damping of translation is modeled by adding damping terms $\eta\,\partial x/\partial t$ and $2\eta\,\partial z/\partial t$ to the balance of forces eqs. (S7) and (S8), respectively. The viscosity of the surrounding fluid also induces a viscous torque (per unit width) $\tau \propto \gamma\,\partial\theta/\partial t$ in the balance of angular momentum (S6), whose rotational damping coefficient, $\gamma \propto \ell\, h\, \eta$, is also given by slender-body theory, see e.g. Batchelor [3].

3. Scaling and slender-body approximation ($h/\ell \ll 1$)

We nondimensionalize lengths by ℓ, heights by $\ell^2|\kappa_0|$, masses by $\rho h \ell^2$, times by $(\rho h \ell^4/EI)^{1/2}$, horizontal forces (per unit width) by EI/ℓ^2 and vertical forces (per unit width) by $EI|\kappa_0|/\ell$. To denote dimensionless versions of the variables in our model we use upper case versions of the symbols used to denote the corresponding dimensional quantity, e.g. $S = s/\ell$, $T = t(EI/\rho h\ell^4)^{1/2}$, but $Z = z/(|\kappa_0\ell^2)$ etc. Assuming the slender-body approximation ($h/\ell \ll 1$), the scaled equations for the balance of angular momentum eq. (S6) and the balances of forces eqs. (S7) and (S8), including dissipative terms per §S1 A 2, are:

$$\frac{\partial^2\theta}{\partial S^2} - \frac{\gamma}{(EI\rho h)^{1/2}}\frac{\partial \theta}{\partial T} - \frac{\rho g h \ell^3}{EI}(1-S)\cos\theta - \Lambda_X \sin\theta + \ell|\kappa_0|\Lambda_Z\cos\theta - \ell|\kappa_0|\Lambda_g\cos\theta = 0; \tag{S10}$$

$$\frac{\partial^2 X}{\partial T^2} + \eta\frac{\ell^2}{(EI\rho h)^{1/2}}\frac{\partial X}{\partial T} - \frac{\partial \Lambda_X}{\partial S} = 0, \quad \text{and} \tag{S11}$$

$$\frac{\partial^2 Z}{\partial T^2} + 2\eta\frac{\ell^2}{(EI\rho h)^{1/2}}\frac{\partial Z}{\partial T} - \frac{\partial \Lambda_Z}{\partial S} = 0; \tag{S12}$$

and the boundary conditions (S9):

$$\left.\frac{\partial\theta}{\partial S}\right|_{S=0,1} = \kappa_0\ell \quad \text{and} \quad \Lambda_X(S,T)\Big|_{S=0,1} = 0. \tag{S13}$$

4. Small-slope approximation: linearization

We linearize the balance of angular momentum, eq. (S10), by assuming that all angles are small, i.e. $\theta \approx \ell|\kappa_0|\partial Z/\partial X \ll 1$. We may then approximate $\cos\theta \approx 1$, $\sin\theta \approx \tan\theta = \ell|\kappa_0|\partial Z/\partial X$, $\partial S \approx \partial X$ etc.) We also assume that $\kappa_0\ell \ll 1$ so that the cylindrical cap is shallow and hence that the edges lie at $X = 0,1$ — this is valid near the initial condition when the shell is pushed flat.

$$\frac{\partial^3 Z}{\partial X^3} - \frac{\gamma}{(EI\rho h)^{1/2}}\frac{\partial^2 Z}{\partial T \partial X} - \frac{\rho g h\ell^2}{EI|\kappa_0|}(1-X) + \Lambda_Z - \Lambda_g = 0, \tag{S14}$$

where we have substituted $\Lambda_X = 0$ (which may be derived from eq. (S11), noting that $\partial/\partial S \approx \partial/\partial X$, the inextensibility of the shell, and the boundary conditions eq. (S13)). Differentiating eq. (S14) with respect to X, and substituting $\partial\Lambda_Z/\partial X$ from eq. (S12), we obtain the dynamic beam equation [4]

$$\frac{\partial^4 Z}{\partial X^4} - \Gamma\frac{\partial^3 Z}{\partial X^2 \partial T} + \frac{1}{\beta} + H\frac{\partial Z}{\partial T} + \frac{\partial^2 Z}{\partial T^2} = 0; \tag{S15}$$

where the three dimensionless groups

$$\beta = \frac{EI|\kappa_0|}{\rho g h \ell^2}, \quad H = \frac{2\eta\ell^2}{(EI\rho h)^{1/2}} \quad \text{and} \quad \Gamma = \frac{\gamma}{(EI\rho h)^{1/2}} \tag{S16}$$

measure the relative importance of bending forces to gravitational force, the damping frequency — the relative importance of viscous forces per unit area to bending forces — and the ratio of the viscous torque to restoring torque by the shell's bending stiffness, respectively. By virtue of the slender-body approximation, and recalling that $\gamma \propto \ell\, h\, \eta$ (see § S1 A 2), we have that

$$\frac{\Gamma}{H} \propto \frac{h}{\ell} \ll 1,$$

and hence we neglect the rotational damping in the the dynamic beam equation eq. (S15), which becomes

$$\frac{\partial^4 Z}{\partial X^4} + \frac{1}{\beta} + H\frac{\partial Z}{\partial T} + \frac{\partial^2 Z}{\partial T^2} = 0. \tag{S17}$$

The corresponding linearized boundary conditions to eq. (S13) and the constraint imposed by Λ_g (i.e. $\int_0^1 \mathrm{d}S \sin\theta = 0$) are

$$\left.\frac{\partial^2 Z}{\partial X^2}\right|_{X=0,1} = \frac{\kappa_0}{|\kappa_0|} \quad \text{and} \quad Z(X,T)\Big|_{X=0,1} = 0. \tag{S18}$$

B. Latch and release

We model the latch mechanism and its release as an indenting force $F(T)$ (dimensionless force per unit width, scaled by $EI|\kappa_0|/\ell$) at the center of the shell ($X = 0.5$). Initially, $F(0) \equiv F_0$ and this force keeps the deformed shell confined such that its center and endpoints are at the same height, i.e. $Z = 0$, see fig. (S2). The shell is in equilibrium due to the reaction force R_0 (dimensionless force per unit width, scaled by $EI|\kappa_0|/\ell$) of the substrate on the edges. The equilibrium in the Z direction (assuming the small-slope approximation in eq. (S12) and extending its domain so that the endpoints are included in the balance, i.e. $X \in [0, 1]$) is then

$$\delta(X)\, 2R_0 + \delta(X-1)\, 2R_0 + \delta(X-1/2)\, F_0 - \frac{\partial \Lambda_Z}{\partial X} = 0, \tag{S19}$$

where we have used Dirac delta functions — represented by δ — to introduce the indenting force and the corresponding reaction by the substrate.

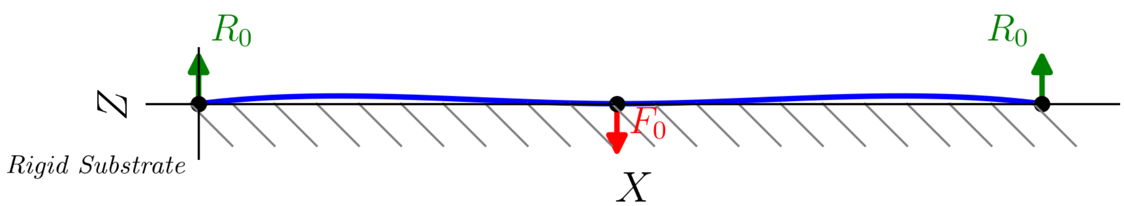

FIG. S2. Schematic representation of the deformed shell by an indenting force F_0 applied at $X = 0$ that serves as a latch.

We break the domain of eq. (S19) in two subdomains: $X_L \in [0, 1/2]$ and $X_R \in [1/2, 1]$. (We use L, R notation to label quantities in each domain.) We obtain from the integral of eq. (S19) over X_L, X_R:

$$\begin{gathered}\Lambda_Z^L(X=0) = -R_0, \quad \Lambda_Z^L(X=1/2) = \frac{1}{2}F_0, \\ \Lambda_Z^R(X=1/2) = -\frac{1}{2}F_0, \quad \text{and} \quad \Lambda_Z^R(X=1) = R_0.\end{gathered} \tag{S20}$$

Next we use these results and the static version of eq. (S14) to evaluate $\partial^3 Z/\partial X^3$ at $X = 1/2^-, 1/2^+$ to obtain that the latch induces a discontinuity of the third derivative at $X = 1/2$:

$$\left[\frac{\partial^3 Z(X,0)}{\partial X^3}\right]_{X=1/2^-}^{X=1/2^+} = F_0. \tag{S21}$$

Therefore, the shape of the shell — when the latch is applied — will be given by the solution of the time-independent version of eq. (S17) with boundary conditions given by eq. (S18) and the latch constraint $Z_0(X = 1/2) = 0$, which we have just seen induces a discontinuity in the third derivative of the shape.

For time $T > 0$ the indenting force is gradually released. We assume a simple model for release with dimensionless characteristic unlatching time τ,

$$F(T) = F_0 \exp(-T/\tau). \tag{S22}$$

The corresponding balance of forces eq. (S12) (assuming again the small-slope approximation and the extended domain, $X \in [0, 1]$) is:

$$\delta(X)\, 2R(T) + \delta(X-1)\, 2R(T) + \delta(X-1/2)\, F(T) + \frac{\partial^2 Z}{\partial T^2} + 2\eta \frac{\ell^2}{(EI\rho h)^{1/2}} \frac{\partial Z}{\partial T} - \frac{\partial \Lambda_Z}{\partial X} = 0, \tag{S23}$$

and hence the discontinuity in the third derivative is now:

$$\left[\frac{\partial^3 Z(X,T)}{\partial X^3}\right]_{X=1/2^-}^{X=1/2^+} = F_0 \exp(-T/\tau). \tag{S24}$$

The latch release phase is thus modelled by the dynamic beam equation eq. (S17) equipped with the set of boundary conditions eq. (S18) and the discontinuity in the third derivative eq. (S24). Initial conditions are provided by the solutions of the static problem, i.e. with the latch applied, and assuming that the shell is at rest when the release phase starts, i.e.

$$\left.\frac{\partial Z}{\partial T}\right|_{T=0} = 0. \tag{S25}$$

In the next section we compute these solutions.

S2. ANALYTIC SOLUTIONS

A. Statics: The shape of a latched shell

1. *Linearized model*

Assuming small deflections, the equilibrium shape of the shell when the latch is applied (see fig. S2) is denoted by $Z_0(X)$ and satisfies a fourth order boundary-value problem

$$\frac{\mathrm{d}^4 Z_0}{\mathrm{d}X^4} + \frac{1}{\beta} = 0, \tag{S26}$$

with boundary conditions $\mathrm{d}^2Z_0/\mathrm{d}^2X(X=0,1) = \kappa_0/|\kappa_0|$ and $Z_0(X=0,1)=0$; the latching constraint is $Z_0(X = 1/2) = 0$, but the force required to achieve this, F_0, is at present unknown. We have seen in § S1 B how the latch constraint induces a discontinuity in the third derivative, Z_0. As noted above, we split the domain of the X coordinates into two: the region to the left of the latch, $X_L \in [0, 1/2]$, and the region to the right, $X_R \in [1/2, 1]$, such that the discontinuity is now at the boundary of each subdomain, and hence we can find a well-behaved function that solves eq. (S26) on each side of the latch. The solution of this system gives the following polynomial for $Z_0(X)$:

$$Z_0(X) = \begin{cases} -\frac{1}{24\beta}X^4 - \frac{1}{2}\left(\frac{\kappa_0}{|\kappa_0|} - \frac{1}{16\beta}\right)X^3 + \frac{1}{2}\frac{\kappa_0}{|\kappa_0|}X^2 - \frac{1}{8}\left(\frac{1}{48}\frac{1}{\beta} + \frac{\kappa_0}{|\kappa_0|}\right)X, & \text{for } X \in [0, 1/2] \\ -\frac{1}{24\beta}\hat{X}^4 + \frac{1}{2}\left(\frac{\kappa_0}{|\kappa_0|} - \frac{1}{16\beta}\right)\hat{X}^3 + \frac{1}{2}\frac{\kappa_0}{|\kappa_0|}\hat{X}^2 + \frac{1}{8}\left(\frac{1}{48}\frac{1}{\beta} + \frac{\kappa_0}{|\kappa_0|}\right)\hat{X}, & \text{for } \hat{X} = X - 1,\ X \in [1/2, 1], \end{cases} \tag{S27}$$

where we have written the solution to the right of the latch as a function of a transformed coordinate $\hat{X}$ that exploits the symmetry of the shell with respect to its center, $X = 1/2$.

2. *Non-linear model*

We complete this section with an analytic solution to the equilibrium, fully non-linear model eqs. (S10), (S11), and (S12) with boundary conditions by eq. (S13). Substituting $\Lambda_X = 0$ (this result follows from the boundary conditions, $\Lambda_X(S)|_{S=0,1} = 0$, combined with the equation $\frac{\mathrm{d}\Lambda_X}{\mathrm{d}S} = 0$, eq. (S11) in equilibrium) into the equilibrium eq. (S10)

$$\frac{\mathrm{d}^2\theta}{\mathrm{d}S^2} - \frac{\rho g h \ell^3}{EI}(1-S)\cos\theta + \ell|\kappa_0|\Lambda_Z\cos\theta - \ell|\kappa_0|\Lambda_g\cos\theta = 0, \tag{S28}$$

where Λ_Z is a constant, yet unknown, by virtue of eq. (S12) in equilibrium. This equation is a non-linear and non-autonomous differential equation that is not solvable analytically for arbitrary values of the parameters $\rho g h\ell^3/EI$ and $\ell|\kappa_0|$ (cf. the equation for a hair strand in Audoly and Pomeau [1]). Yet it can be solved in the limit of weak gravity (i.e. very stiff, very light and/or very short shell) for which we do not need a force (i.e. the Lagrange multiplier Λ_g) to constrain the position of the edges, and the equation (S28) becomes

$$\frac{\mathrm{d}^2\theta}{\mathrm{d}S^2} + \ell|\kappa_0|\Lambda_Z\cos\theta = 0, \tag{S29}$$

with moment-free boundary conditions at $S = 0, 1$:

$$\left.\frac{\mathrm{d}\theta}{\mathrm{d}S}\right|_{S=0,1} = \ell\kappa_0. \tag{S30}$$

Invoking the same arguments as in §S1 B, we notice that Λ_Z accounts for the vertical forces by the latch mechanism and the corresponding reaction from the substrate. Therefore, by integrating eq. (S29) along the two subdomains $S_L \in [0, 1/2]$ and $S_R \in [1/2, 1]$ we obtain

$$\Lambda_Z^L(S=0) = -R_0, \quad \Lambda_Z^L(S=1/2) = \frac{1}{2}F_0,$$
$$\Lambda_Z^R(S=1/2) = -\frac{1}{2}F_0, \quad \text{and} \quad \Lambda_Z^R(S=1) = R_0, \tag{S31}$$

and hence $\theta(S)$ exhibits a discontinuity in the second derivative due to the latch force, i.e. combining eqs. (S29) and (S31) we get:

$$\left[\frac{\mathrm{d}^2\theta}{\mathrm{d}S^2}\right]_{S=1/2^-}^{S=1/2^+} = F_0. \tag{S32}$$

Λ_Z (and hence F_0) on each side of the latch are given now by the non-linear constraints

$$\int_0^{1/2} \sin\theta(S)\,\mathrm{d}S = 0, \quad \text{and} \quad \int_{1/2}^{1} \sin\theta(S)\,\mathrm{d}S = 0. \tag{S33}$$

The integral of eq. (S29) can be expressed in elliptic-function form [1]:

$$\theta_L^{\pm}(S, \Lambda_L, \theta_0, \ell, \kappa_0) = \frac{\pi}{2} - 2\,\mathrm{am}\left(\mathcal{F}\left(\frac{\pi - 2\theta_0}{4}, k_L\right) \pm \frac{1}{2}\sqrt{\Delta_L}\, S,\ k_L\right) \quad \text{for } S \in [0, 1/2] \tag{S34}$$

$$\theta_R^{\pm}(S, \Lambda_R, \theta_1, \ell, \kappa_0) = \frac{\pi}{2} - 2\,\mathrm{am}\left(\mathcal{F}\left(\frac{\pi - 2\theta_1}{4}, k_R\right) \pm \frac{1}{2}\sqrt{\Delta_R}\,(S-1),\ k_R\right) \quad \text{for } S \in [1/2, 1], \tag{S35}$$

where $\mathrm{am}(\cdot, k)$ is the Jacobi amplitude function, $\mathcal{F}(\phi, k)$ is the incomplete elliptic integral of the first kind, $\theta_{(0,1)}$ is the angle at the edges, and

$$k_L = \frac{-4\ell|\kappa_0|\Lambda_Z^L}{(\kappa_0\ell)^2 - 2\ell|\kappa_0|\Lambda_Z^L + 2\ell|\kappa_0|\Lambda_Z^L\sin(\theta_0)},$$
$$k_R = \frac{-4\ell|\kappa_0|\Lambda_Z^R}{(\kappa_0\ell)^2 - 2\ell|\kappa_0|\Lambda_Z^R + 2\ell|\kappa_0|\Lambda_Z^R\sin(\theta_1)},$$
$$\Delta_L = (\kappa_0\ell)^2 - 2\ell|\kappa_0|\Lambda_Z^L + 2\ell|\kappa_0|\Lambda_Z^L\sin(\theta_0),$$
$$\Delta_R = (\kappa_0\ell)^2 - 2\ell|\kappa_0|\Lambda_Z^R + 2\ell|\kappa_0|\Lambda_Z^R\sin(\theta_1).$$

We have 4 solutions (S34), (S35) containing 4 unknown constants $(\theta_0, \theta_1, \Lambda_Z^L, \Lambda_Z^R)$ that we will determine by satisfying the boundary conditions (S30) and the constraints (S33).

To integrate the constraints in eq. (S33) we follow the same steps as Wagner and Vella [5]: considering the example of θ_L, we first change variables

$$\int_0^{1/2} \mathrm{d}S\, \sin\theta_L(S) = \int_{\theta_0}^{\theta_{1/2}} \mathrm{d}\theta_L \left(\frac{\mathrm{d}\theta_L}{\mathrm{d}S}\right)^{-1} \sin\theta_L,$$

for which

$$\frac{\mathrm{d}\theta_L}{\mathrm{d}S} = \pm\left[2\left(\frac{1}{2} + \ell|\kappa_0|\Lambda_Z^L\sin\theta_0 - \ell|\kappa_0|\Lambda_Z^L\sin\theta_L\right)\right]^{1/2}$$

is defined up to a sign. We then split the integral into two

$$\int_{\theta_0}^{\theta_{1/2}} \mathrm{d}\theta_L \left(\frac{\mathrm{d}\theta_L}{\mathrm{d}S}\right)^{-1} \sin\theta_L = -\int_{\theta_0}^{\theta_S} \mathrm{d}\theta_L \left(\frac{\mathrm{d}\theta_L}{\mathrm{d}S}\right)^{-1} \sin\theta_L + \int_{\theta_S}^{\theta_{1/2}} \mathrm{d}\theta_L \left(\frac{\mathrm{d}\theta_L}{\mathrm{d}S}\right)^{-1} \sin\theta_L,$$

where θ_S is the angle at $S = S_0$, with S_0 such that $\frac{\mathrm{d}\theta_L}{\mathrm{d}S}\big|_{S=S_0} = 0$, and we have introduced the sign of the first derivative explicitly. The integral constraints (S33) are then

$$\begin{aligned}
&\mathrm{C}_L(\theta_0, S_0, \Lambda_Z^L, \ell, \kappa_0) = \\
&\quad \frac{1}{\ell|\kappa_0|\Lambda_Z^L}\Bigg[\sqrt{\Delta_L}\left(\mathcal{E}\left(\tfrac{1}{4}(\pi - 2\theta_0), k_L\right) - 2\mathcal{E}\left(\tfrac{1}{4}(\pi - 2\theta_L^+(S_0)), k_L\right) + \mathcal{E}\left(\tfrac{1}{4}(\pi - 2\theta_L^+(1/2)), k_L\right)\right) \\
&\quad - \frac{(\kappa_0\ell)^2 + 2\ell|\kappa_0|\Lambda_Z^L \sin(\theta_0)}{\sqrt{\Delta_L}}\left(\mathcal{F}\left(\tfrac{1}{4}(\pi - 2\theta_0), k_L\right) - 2\mathcal{F}\left(\tfrac{1}{4}(\pi - 2\theta_L^+(S_0)), k_L\right)\right. \\
&\quad \left.+\mathcal{F}\left(\tfrac{1}{4}(\pi - 2\theta_L^+(1/2)), k_L\right)\right)\Bigg], \quad \text{and}
\end{aligned} \tag{S36}$$

$$\begin{aligned}
&\mathrm{C}_R(\theta_1, S_0, \Lambda_Z^R, \ell, \kappa_0) = \\
&\quad \frac{1}{\ell|\kappa_0|\Lambda_Z^R}\Bigg[\sqrt{\Delta_R}\left(-\mathcal{E}\left(\tfrac{1}{4}(\pi - 2\theta_1), k_R\right) + 2\mathcal{E}\left(\tfrac{1}{4}(\pi - 2\theta_R^-(S_0)), k_R\right) - \mathcal{E}\left(\tfrac{1}{4}(\pi - 2\theta_R^-(1/2)), k_R\right)\right) \\
&\quad - \frac{(\kappa_0\ell)^2 + 2\ell|\kappa_0|\Lambda_Z^R \sin(\theta_1)}{\sqrt{\Delta_R}}\left(-\mathcal{F}\left(\tfrac{1}{4}(\pi - 2\theta_1), k_R\right) + 2\mathcal{F}\left(\tfrac{1}{4}(\pi - 2\theta_R^-(S_0)), k_R\right)\right. \\
&\quad \left.-\mathcal{F}\left(\tfrac{1}{4}(\pi - 2\theta_R^-(1/2)), k_R\right)\right)\Bigg],
\end{aligned} \tag{S37}$$

where $\mathcal{E}(\phi, k)$ is the incomplete elliptic integral of the second kind.

Finally, we compute numerically the six unknowns $(\theta_0, \theta_1, \Lambda_Z^L, \Lambda_Z^R, S_0^L, S_0^R)$ from the system of six equations:

$$\begin{cases}
\left(\theta_R^- - \theta_L^+\right)\big|_{S=1/2} = 0, \\
\left(\frac{\mathrm{d}\theta_R^+}{\mathrm{d}S} - \frac{\mathrm{d}\theta_L^+}{\mathrm{d}S}\right)\Big|_{S=1/2} = 0, \\
\mathrm{C}_L(\theta_0, S_0^L, \Lambda_Z^L, \ell, \kappa_0) = 0 \\
\mathrm{C}_R(\theta_1, S_0^R, \Lambda_Z^R, \ell, \kappa_0) = 0 \\
\frac{\mathrm{d}\theta_L^+}{\mathrm{d}S}\Big|_{S=S_0^L} = 0, \\
\frac{\mathrm{d}\theta_R^+}{\mathrm{d}S}\Big|_{S=S_0^R} = 0.
\end{cases} \tag{S38}$$

In fig. (3) of the main text we plot the latch force $\Lambda_Z^R - \Lambda_Z^L$ (cf. eq. (S32)) using the values for Λ_Z^L, Λ_Z^R obtained by solving this system numerically.

B. Dynamic beam equation: the latch is released

The dynamic beam equation (S17) with the boundary, initial and continuity conditions discussed above can be solved analytically by letting

$$Z(X,T) = \zeta(X,T) - w(X) - \exp(-T/\tau)\, y(X), \tag{S39}$$

where $\zeta(X,T)$ is the separable solution of the homogeneous problem, $w(X)$ is a particular solution that absorbs the inhomogeneous parts arising from the natural curvature, and $y(X)$ is a particular solution that absorbs the discontinuity imposed by eq. (S24). Specifically, we find that

$$w(X) = \frac{1}{2}\left[\frac{1}{12}\frac{1}{\beta}X^4 - \frac{1}{6}\frac{1}{\beta}X^3 - \frac{\kappa_0}{|\kappa_0|}X^2 + \left(\frac{1}{12}\frac{1}{\beta} + \frac{\kappa_0}{|\kappa_0|}\right)X\right], \tag{S40}$$

while

$$y(x) = \begin{cases} y_L(X), \quad \text{for} \quad X \in [0, 1/2] \\ -y_L(\hat{X}),\ \hat{X} = X - 1, \quad \text{for} \quad X \in [1/2, 1]; \end{cases} \tag{S41}$$

with

$$y_L(X) = \left[\frac{\mathrm{d}^3 Z_0(X)}{\mathrm{d}X^3}\right]_{X=1/2^-}^{X=1/2^+} \left(\frac{\tau}{2}\right)^{3/2} \frac{1}{(1-H\tau)^{3/4}} \left\{ c_1^L \sinh\left[\frac{(1-H\tau)^{1/4}}{\sqrt{2\tau}} X\right] \cos\left[\frac{(1-H\tau)^{1/4}}{\sqrt{2\tau}} X\right] \right.$$
$$\left. + c_2^L \cosh\left[\frac{(1-H\tau)^{1/4}}{\sqrt{2\tau}} X\right] \sin\left[\frac{(1-H\tau)^{1/4}}{\sqrt{2\tau}} X\right] \right\}, \tag{S42}$$

for $H\tau < 1$ (i.e. rapid release compared to the intrinsic damping scale, $1/H$). Here, c_1^L, c_2^L are the constants:

$$c_1^L = -\frac{\cosh \frac{(1-H\tau)^{1/4}}{2\sqrt{2\tau}} \cos \frac{(1-H\tau)^{1/4}}{2\sqrt{2\tau}} + \sinh \frac{(1-H\tau)^{1/4}}{2\sqrt{2\tau}} \sin \frac{(1-H\tau)^{1/4}}{2\sqrt{2\tau}}}{\cosh^2 \frac{(1-H\tau)^{1/4}}{2\sqrt{2\tau}} \cos^2 \frac{(1-H\tau)^{1/4}}{2\sqrt{2\tau}} + \sinh^2 \frac{(1-H\tau)^{1/4}}{2\sqrt{2\tau}} \sin \frac{(1-H\tau)^{1/4}}{2\sqrt{2\tau}}}, \tag{S43}$$

$$c_2^L = \frac{\cosh \frac{(1-H\tau)^{1/4}}{2\sqrt{2\tau}} \cos \frac{(1-H\tau)^{1/4}}{2\sqrt{2\tau}} - \sinh \frac{(1-H\tau)^{1/4}}{2\sqrt{2\tau}} \sin \frac{(1-H\tau)^{1/4}}{2\sqrt{2\tau}}}{\cosh^2 \frac{(1-H\tau)^{1/4}}{2\sqrt{2\tau}} \cos^2 \frac{(1-H\tau)^{1/4}}{2\sqrt{2\tau}} + \sinh^2 \frac{(1-H\tau)^{1/4}}{2\sqrt{2\tau}} \sin \frac{(1-H\tau)^{1/4}}{2\sqrt{2\tau}}}. \tag{S44}$$

For completeness, we note that the separable solution is:

$$\zeta(X,T) = e^{-\frac{H}{2}T} \sum_{n=1}^{\infty} \sin(n\pi X)\, A_n \cos(\omega_n T + \varphi_n), \tag{S45}$$

where $\omega_n = \frac{H}{2}\left(\frac{4n^4\pi^4}{H^2} - 1\right)^{1/2}$ are the frequencies of natural oscillations in underdamped conditions ($H < 2n^2\pi^2$). The φ_n are phase differences determined from the initial conditions, which are now written as $\zeta(X,0) = Z_0(X) + w(X) + y(X)$ and, using (S25), we have

$$\left.\frac{\partial \zeta}{\partial T}\right|_{T=0} = -\frac{y(X)}{\tau}.$$

The constants A_n and φ_n are

$$A_n = \mathrm{sgn}\,(a_n)\sqrt{a_n^2 + b_n^2} \quad \text{and} \quad \varphi_n = \arctan\left(\frac{-b_n}{a_n}\right), \tag{S46}$$

where a_n, b_n are the coefficients of the Fourier sine series of the relevant initial conditions, i.e.

$$\begin{aligned} a_n =& 2\int_0^1 \mathrm{d}X\, \zeta(X,0) \sin n\pi X \\ =& 2\left[\frac{\mathrm{d}^3 Z_0(X)}{\mathrm{d}X^3}\right]_{X=1/2^-}^{X=1/2^+} \frac{1}{1+\frac{n^4\pi^4\tau^2}{1-H\tau}} \frac{1}{n^4\pi^4} \sin n\frac{\pi}{2}, \end{aligned} \tag{S47}$$

$$\begin{aligned} b_n =& \frac{2}{(n\pi)^2}\int_0^1 \mathrm{d}X\, \frac{\partial \zeta}{\partial T}(X,0) \sin n\pi X \\ =& \frac{1}{\omega_n}\left[\frac{\mathrm{d}^3 Z_0(X)}{\mathrm{d}X^3}\right]_{X=1/2^-}^{X=1/2^+} \frac{1}{1+\frac{n^4\pi^4\tau^2}{1-H\tau}} \frac{1}{n^4\pi^4} \sin n\frac{\pi}{2} \left[\frac{H}{2} + \frac{n^4\pi^4\tau}{1-H\tau}\right]. \end{aligned} \tag{S48}$$

1. *Slow release ($H\tau \geq 1$)*

We include for completeness the analytic results of the dynamic beam equation (S17) when the unlatching timescale τ is larger than the damping timescale H^{-1} — yet $H < 2\pi^2$ and hence all modes are oscillating. For $H\tau > 1$, the solution is given by eq. (S39) with $w(X)$ from eq. (S40) and $\zeta(X,T)$ from eq. (S45) (with the same constants as in eqs. (S46), (S47) and (S48)). $y(X)$ is as it is defined in eq. (S41) with $y_L(X)$:

$$y_L(X) = \left[\frac{\mathrm{d}^3 Z_0(X)}{\mathrm{d}X^3}\right]_{X=1/2^-}^{X=1/2^+} \frac{\tau^{3/2}}{4} \frac{1}{(H\tau-1)^{3/4}} \left\{ \frac{\sinh\left[\frac{(H\tau-1)^{1/4}}{\sqrt{\tau}} X\right]}{\cosh\left[\frac{(H\tau-1)^{1/4}}{2\sqrt{\tau}}\right]} - \frac{\sin\left[\frac{(H\tau-1)^{1/4}}{\sqrt{\tau}} X\right]}{\cos\left[\frac{(H\tau-1)^{1/4}}{2\sqrt{\tau}}\right]} \right\}. \tag{S49}$$

For $H\tau = 1$ the solution is also constructed as in eq. (S39), with $w(X)$ given by eq. (S40), $y(X)$ by eq. (S41), where $y_L(X)$ is

$$y_L(X) = \frac{1}{4}\left[\frac{\mathrm{d}^3 Z_0(X)}{\mathrm{d}X^3}\right]_{X=1/2^-}^{X=1/2^+}\left(\frac{1}{3}X^3 - \frac{1}{4}X\right), \tag{S50}$$

and the separable solution $\zeta(X,T)$ is given by

$$\zeta(X,T) = 4\left[\frac{\mathrm{d}^3 Z_0(X)}{\mathrm{d}X^3}\right]_{X=1/2^-}^{X=1/2^+} e^{-\frac{T}{2\tau}}\sum_{n=1}^{\infty}\frac{\sin n\frac{\pi}{2}}{(n\pi)^4(4\tau^2 n^4\pi^4 - 1)^{1/2}}\sin(n\pi X)\sin(\omega_n T), \tag{S51}$$

with the frequencies of natural oscillations now given by $\omega_n = \frac{1}{2\tau}\left(4n^4\pi^4\tau^2 - 1\right)^{1/2}$.

S3. JUMPING BEHAVIOR

A. Reaction force at $X = 0$

We analyze the jumping behavior in terms of the three dimensionless parameters in the model: β, τ and H. We begin by noting that the scaled reaction force of the substrate on the edge of the shell, $R(T)$, may be calculated from the solution $Z(X,T)$, eq. (S39), as

$$R(T) = \left.\frac{\partial^3 Z}{\partial X^3}\right|_{X=0}. \tag{S52}$$

This result follows from evaluating eq. (S14) at $X = 0$ and substituting the result $\Lambda_Z(0,T) = -R(T)$, obtained from the integral of eq. (S23).

The reaction force can only be positive — if it becomes negative then the shell has lost contact with the ground, and the shell has jumped. Finding the smallest positive root of $R(T) = 0$ therefore determines the jumping time, T_{jump}. The analytic expressions of the force at $X = 0$ for the different solutions in § S2 are:

$$R(0,T) = \begin{cases} \frac{1}{2\beta} - \left[\frac{\mathrm{d}^3 Z_0(X)}{\mathrm{d}X^3}\right]_{X=1/2^-}^{X=1/2^+}\left\{\sum_{n=1}^{\infty}\frac{2}{1+\frac{n^4\pi^4\tau^2}{1-H\tau}}\frac{1}{n\pi}\sin\left(n\frac{\pi}{2}\right)e^{-\frac{H}{2}T}\left[\cos\omega_n T + \frac{1}{\omega_n}\left(\frac{H}{2} + \frac{n^4\pi^4\tau}{1-H\tau}\right)\sin\omega_n T\right]\right. \\ \qquad \left. +\frac{1}{2}e^{-\frac{T}{\tau}}\frac{\cosh\frac{(1-H\tau)^{1/4}}{2\sqrt{2\tau}}\cos\frac{(1-H\tau)^{1/4}}{2\sqrt{2\tau}}}{\cosh^2\frac{(1-H\tau)^{1/4}}{2\sqrt{2\tau}}\cos^2\frac{(1-H\tau)^{1/4}}{2\sqrt{2\tau}}+\sinh^2\frac{(1-H\tau)^{1/4}}{2\sqrt{2\tau}}\sin^2\frac{(1-H\tau)^{1/4}}{2\sqrt{2\tau}}}\right\}, & \text{for } H\tau < 1; \\ \frac{1}{2\beta} - \left[\frac{\mathrm{d}^3 Z_0(X)}{\mathrm{d}X^3}\right]_{X=1/2^-}^{X=1/2^+}\left[\frac{1}{2}e^{-\frac{T}{\tau}} + 4e^{-\frac{T}{2\tau}}\sum_{n=1}^{\infty}\frac{\sin n\frac{\pi}{2}}{n\pi(4\tau^2 n^4\pi^4-1)^{1/2}}\sin\omega_n T\right], & \text{for } H\tau = 1; \\ \frac{1}{2\beta} - \left[\frac{\mathrm{d}^3 Z_0(X)}{\mathrm{d}X^3}\right]_{X=1/2^-}^{X=1/2^+}\left\{e^{-\frac{H}{2}T}\sum_{n=1}^{\infty}\frac{4\sin n\frac{\pi}{2}}{n\pi(4\tau^2 n^4\pi^4-1)^{1/2}}\sin\omega_n T\right. \\ \qquad \left. +e^{\frac{-T}{\tau}}\frac{1}{4}\left[\frac{1}{\cosh\frac{(H\tau-1)^{1/4}}{2\sqrt{\tau}}} + \frac{1}{\cos\frac{(H\tau-1)^{1/4}}{2\sqrt{\tau}}}\right]\right\}, & \text{for } H\tau > 1. \end{cases} \tag{S53}$$

Recall that the natural frequencies are $\omega_n = \frac{H}{2}\left(\frac{4n^4\pi^4}{H^2} - 1\right)^{1/2}$ for $H\tau \neq 1$, and $\omega_n = \frac{1}{2\tau}\left(4n^4\pi^4\tau^2 - 1\right)^{1/2}$ for $H\tau = 1$.

B. Phase diagram

We sample a grid of points (β, τ, H) in the phase space and find for each of them the roots of $R(T)$ in eq. (S53) numerically with the *Chebfun* package [6] in *Matlab*. For this computation the series eq. (S53) is truncated at mode $n_{\text{modes}} = \left\lceil\sqrt{2/(\pi\tau)}\right\rceil$, given by the condition that the smallest time that we resolve compares with τ, i.e. $\left(\omega_{n_{\text{modes}}}\right)^{-1} \sim \tau$. This choice can be justified with the physical argument that higher modes should be supressed by the external force due to the latch-release mechanism. We record the time of jumping T_{jump} and normalize it with the period of the fundamental mode $T_1 = 2\pi/\omega_1$. We show the results for $H = 0$ and $H = 0.01$ in fig. S3.

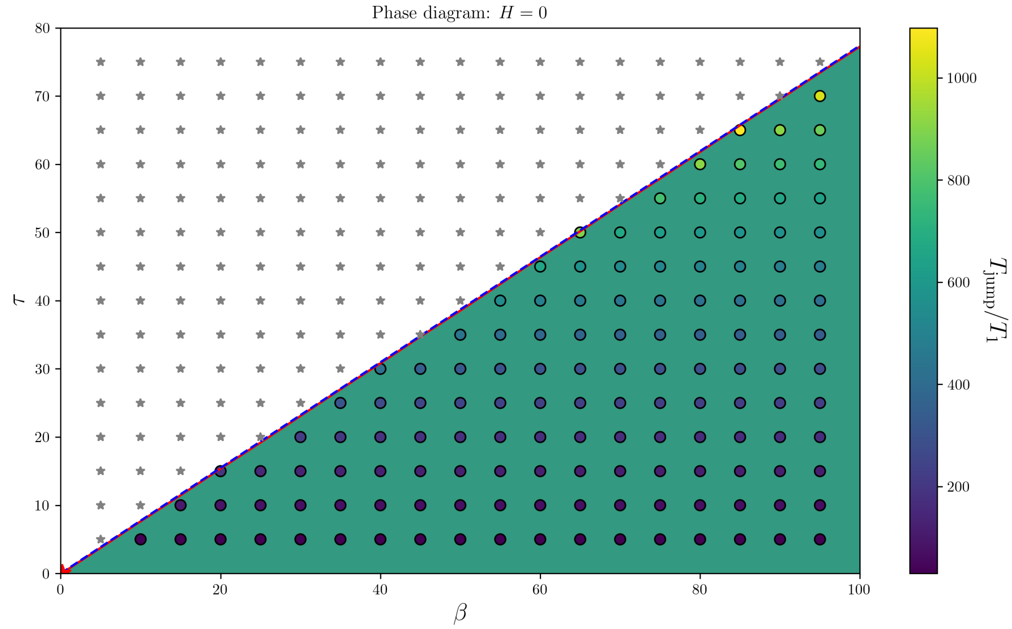

(a)

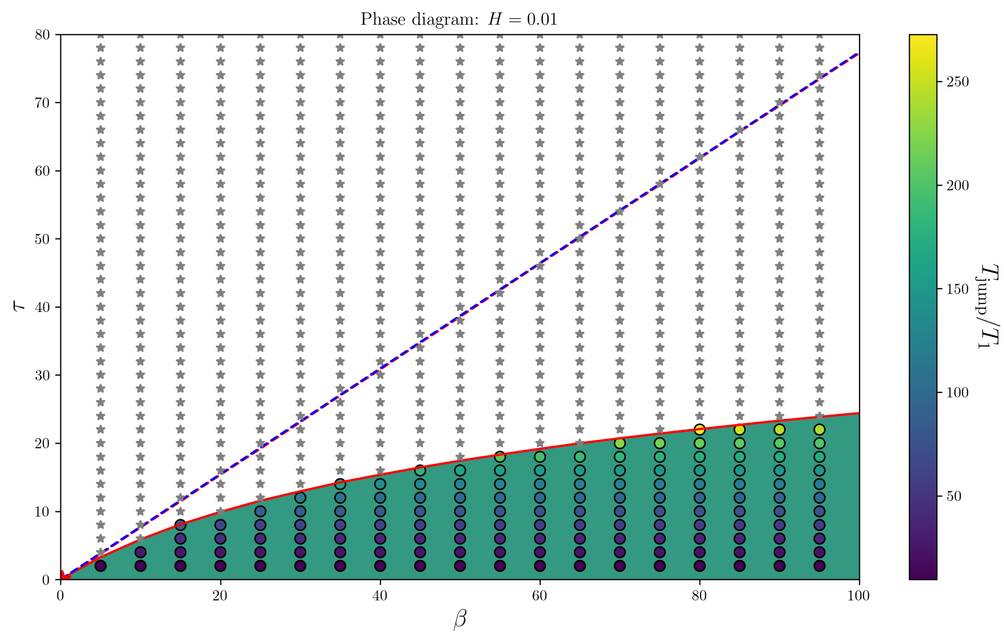

(b)

FIG. S3. Phase diagram of the jumping behavior of a curved shell on a flat surface at different values of the damping $H = 0$ (a), and $H = 0.01$ (b). The jumping behavior of the shell is characterized by the triad (β, τ, H): there is a jumping phase (shaded in green) and a non-jumping phase (shaded in white). Grey stars indicate failed attempts and dots indicate jumps with jumping time $T_{\rm jump}$ given by the color bar to the right. The asymptotic expression for the phase boundary eq. (S55) is plotted with a blue dashed line.

1. *Asymptotic expressions of the phase boundary*

Having computed the phase boundaries in fig. S3 numerically, we now seek an asymptotic approximation of the force at the origin eq. (S53) that will allow us to determine asymptotic results for the phase boundary and $\beta_{\rm crit}$, which is the minimal β needed for jumping.

We start by considering the asymptotic limit of $H \ll 1$ (undamped), slow release $\tau \gg 1$ and large time $T \gg \tau$ for a light shell ($\beta \gg 1$) in $R(0,T)$ with $H\tau < 1$ using eq. (S53):

$$R(0,T) \approx \frac{1}{2\beta} + 6\sum_{n=1}^{\infty} \frac{2\sin\left(n^2\pi^2 T\right)}{n^3\pi^3\tau} \sin\left(n\frac{\pi}{2}\right). \tag{S54}$$

Here we have used the asymptotic limit of $\beta \gg 1$ for the discontinuity in the third derivative of the statics $Z_0(X)$ from eq. (S27). This limit accounts for the largest τ (slowest release) for which jumping occurs — considering otherwise the most favorable conditions for jumping for β and H, i.e. a light object with no damping. The condition for no jumping corresponds to when the series attains a local minimum and $R(0,T) = 0$. A good estimate of this behavior is given by the local minimum of the main mode ($n = 1$), and hence we assume $\sin(\pi^2 T) = -1$ in eq. (S54). The condition $R(0,T) = 0$ then poses a linear equation for τ that we can solve, and we obtain

$$\tau_{\text{boundary}}(\beta) = \frac{24}{\pi^3}\beta. \tag{S55}$$

We now examine the opposite limit of quick release $\tau \ll 1$ and heavy shell (i.e. small β); the asymptotic expression for $R(0,T)$ eq. (S53) is, assuming again a large time $T \gg \tau$ and $H \ll 1$, given by

$$R(0,T,n_{\text{modes}}) \approx \frac{1}{2\beta} - \left[\frac{\mathrm{d}^3 Z_0(X)}{\mathrm{d}X^3}\right]_{X=1/2^-}^{X=1/2^+} \sum_{n=1}^{n_{\text{modes}}} \frac{2\cos\left(n^2\pi^2 T\right)}{n\pi} \sin\left(n\frac{\pi}{2}\right), \tag{S56}$$

where we have assumed $n_{\text{modes}}^4 \pi^4 \tau^2 \ll 1$. We will further approximate $R(0,T,n_{\text{modes}})$ by truncating the series at the main mode ($n = 1$). The condition of no jump is then given by

$$R(0,T,1) - \max_T |R(0,T,n_{\text{modes}}) - R(0,T,1)| = 0, \tag{S57}$$

where we have subtracted the maximum amplitude of the residual series after removing the fundamental mode. To estimate this amplitude, we will use the fact that it is bounded by the root mean square (RMS) amplitude of the residual series. Given that the series in eq. (S56) converges and the basis functions $\cos(n^2\pi^2 T)$ are bounded and quasi-orthogonal, we can calculate the RMS amplitude

$$\text{RMS}^2[R(0,T,n_{\text{modes}}) - R(0,T,1)] \approx \frac{1}{2}\left\{\frac{2}{\pi}\left[\frac{\mathrm{d}^3 Z_0(X)}{\mathrm{d}X^3}\right]_{X=1/2^-}^{X=1/2^+}\right\}^2 \sum_{n=3,\, n\ \text{odd}}^{\infty} \frac{1}{n^2}. \tag{S58}$$

Applying the well known result

$$\sum_{n=1,\, n\ \text{odd}}^{\infty} \frac{1}{n^2} = \frac{\pi^2}{8},$$

we obtain

$$\text{RMS}^2[R(0,T,n_{\text{modes}}) - R(0,T,1)] \approx \frac{1}{2}\left\{\frac{2}{\pi}\left[\frac{\mathrm{d}^3 Z_0(X)}{\mathrm{d}X^3}\right]_{X=1/2^-}^{X=1/2^+}\right\}^2 \left(\frac{\pi^2}{8} - 1\right). \tag{S59}$$

We estimate from our numerical solutions that the critical value for jumping is $\beta \approx 0.2$ (see fig. 2b in the main text). We then estimate the discontinuity in the third derivative for this value of β (using eq. (S27)) and find that $\text{RMS}[R(0,T,n_{\text{modes}}) - R(0,T,1)] \sim 1$; thus can we rewrite the condition of no jump eq. (S57) as

$$R(0,T,1) - 1 = 0. \tag{S60}$$

We solve this equation and obtain

$$\beta_{\text{crit}} = \frac{5 + 2\pi}{4(12+\pi)} \approx 0.186. \tag{S61}$$

We plot this estimate for β_{crit} in fig. 2b in the main text, and note that the approximate value in (S61) is consistent with our numerical results obtained without this truncation.

C. Efficiency of jumping

We define the efficiency of jumping as the ratio of translational kinetic energy at the point of jumping, K_{trans}, to the stored energy E_0. Here, E_0 is the sum of the bending and gravitational potential energy of the latched shell, i.e. for the solution in eq. (S27),

$$E_0(\beta) = \frac{1}{2}\left[\int_0^1 \mathrm{d}X \left(\frac{\mathrm{d}^2 Z_0}{\mathrm{d}X^2} - \frac{\kappa_0}{|\kappa_0|}\right)^2\right] + \frac{1}{\beta}\int_0^1 \mathrm{d}X\, Z_0 = \frac{-3+160\beta(1+72\beta)}{30720\beta^2}; \tag{S62}$$

the translational kinetic energy is

$$K_{\mathrm{trans}} = \frac{1}{2}\left[\frac{\partial}{\partial T}\int_0^1 \mathrm{d}X\, Z(X,T)\right]^2, \tag{S63}$$

directly from the solution in (S39).

In fig. 4 of the main text there are certain *pessimal* values of τ for which the efficiency drops dramatically. We notice that these pessimal values correspond to when τ is close to those jumping times T_{jump} such that $R(T_{\mathrm{jump}})$ is a local minimum. In this case, the shell is experiencing a very weak reaction force for a 'long time' before jumping — when jumping happens otherwise (i.e. away from the minima of $R(T)$) the force changes rapidly and hence, while $R(T) = 0$ denotes the moment of jumping, the shell experiences larger forces closer to jumping.

To estimate these pessimal values we need to find the local minima in the oscillating part of $R(T)$ from eq. (S53) ($H\tau < 1$). Truncating $R(T)$ at the fundamental mode, the first minimum is located at approximately

$$T \approx \frac{3}{2}\frac{\pi}{\omega_1}. \tag{S64}$$

The accuracy of this result increases as τ increases. The first pessimal value is thus given by the roots of $R(T = \frac{3}{2}\frac{\pi}{\omega_1})$ — as given by eq. (S53) with the series truncated at the main mode, and considering the asymptotic limit $\tau \gg 1$, we find

$$\begin{aligned} R\left(\frac{3}{2}\frac{\pi}{\omega_1}\right) \approx & \frac{1}{2\beta} - \left[\frac{\mathrm{d}^3 Z_0(X)}{\mathrm{d}X^3}\right]_{X=1/2^-}^{X=1/2^+} \left\{\frac{-2\pi^4\tau}{\pi(1+\pi^4\tau^2)\omega_1} e^{-\frac{3\pi H}{4\omega_1}}\right. \\ & \left. + \frac{1}{2} e^{-\frac{3\pi}{2\omega_1\tau}} \frac{\cosh\frac{(1-H\tau)^{1/4}}{2\sqrt{2\tau}}\cos\frac{(1-H\tau)^{1/4}}{2\sqrt{2\tau}}}{\cosh^2\frac{(1-H\tau)^{1/4}}{2\sqrt{2\tau}}\cos^2\frac{(1-H\tau)^{1/4}}{2\sqrt{2\tau}} + \sinh^2\frac{(1-H\tau)^{1/4}}{2\sqrt{2\tau}}\sin^2\frac{(1-H\tau)^{1/4}}{2\sqrt{2\tau}}}\right\} \\ & = 0. \end{aligned} \tag{S65}$$

Successive pessimal values are obtained by solving eq. (S65) evaluated at $T = \frac{7}{2}\frac{\pi}{\omega_1}, \frac{11}{2}\frac{\pi}{\omega_1}, \frac{15}{2}\frac{\pi}{\omega_1}, \ldots$. Fig. S4 shows these for $\beta = 1, 10$, and $H = 0.1$.

D. Larval Beetles

1. *Parameter Values*

We measured the radius of curvature of the larval beetles by fitting a circle to their bodies in the video from Bertone *et al.* [7], see fig. S5. We calculate an estimated radius of approximately 0.6 mm ($|\kappa_0^{\max}| \approx 1.69\ \mathrm{mm}^{-1}$).

From these videos, we also measure a curling time scale $t_{\mathrm{curl}} \approx 44$ ms. We then estimate the bending stiffness $B = EI$ using t_{curl} and the measured curvature [8]

$$B = (t_{\mathrm{curl}})^{-2}(\kappa_0)^{-4}\rho, \tag{S66}$$

and obtain an estimate value for the Young's modulus (taking $h \sim 0.6$ mm $\rho \sim mh^{-2}\ell$ with $m \sim 1.3\,10^{-6}$ kg, $\ell \sim 6$ mm from Bertone *et al.* [7])

$$E \sim 10\ \mathrm{kPa}.$$

Also, we estimate that

$$\beta \sim 1$$

for these results.

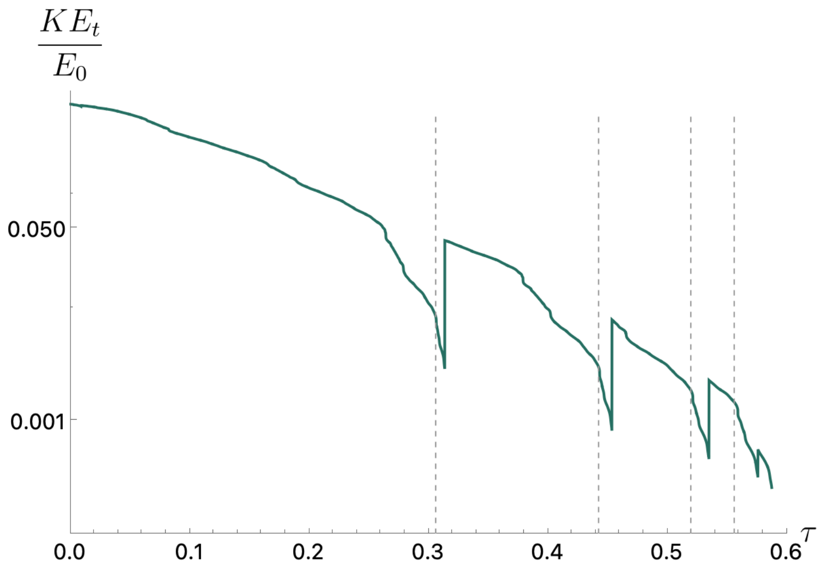

(a)

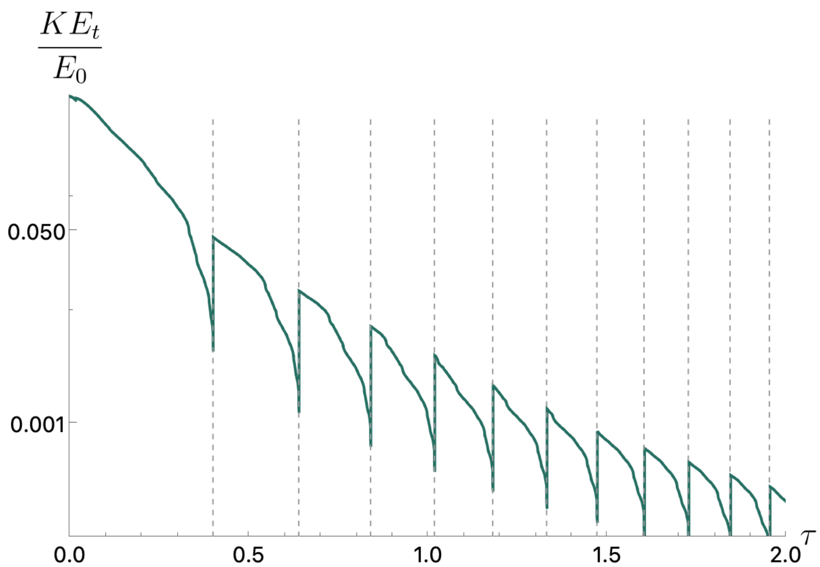

(b)

FIG. S4. Efficiency of jumping for for $\beta = 1$ in panel (a), and $\beta = 10$ in panel (b); $H = 0.1$ for both (a) and (b). Predicted pessimal values of τ from the numerical roots of eq. (S65) are plotted as vertical dashed lines.

2. Stored Energy

To examine in the main text the attaching force of the larval beetles (see fig. 3 in the main text, with dimensions as per the results in the previous section). We complement this exploration with the analysis of the stored energy (gravitational+bending) by the larval beetles as a function of the curvature. We plot the results using the linearized model eq. (S62) in fig. S6. We also include the results for the non-linear model (see §S2 A 2), for which the energy is

$$E_0(\beta, \ell, \kappa_0) = \frac{EI}{\ell}\left[E_0^b(\ell, \kappa_0) + \frac{\kappa_0^2 \ell}{\beta} 2\int_0^{1/2} \mathrm{d}S\, Z_0^{L,\mathrm{nonlinear}}\right]; \tag{S67}$$

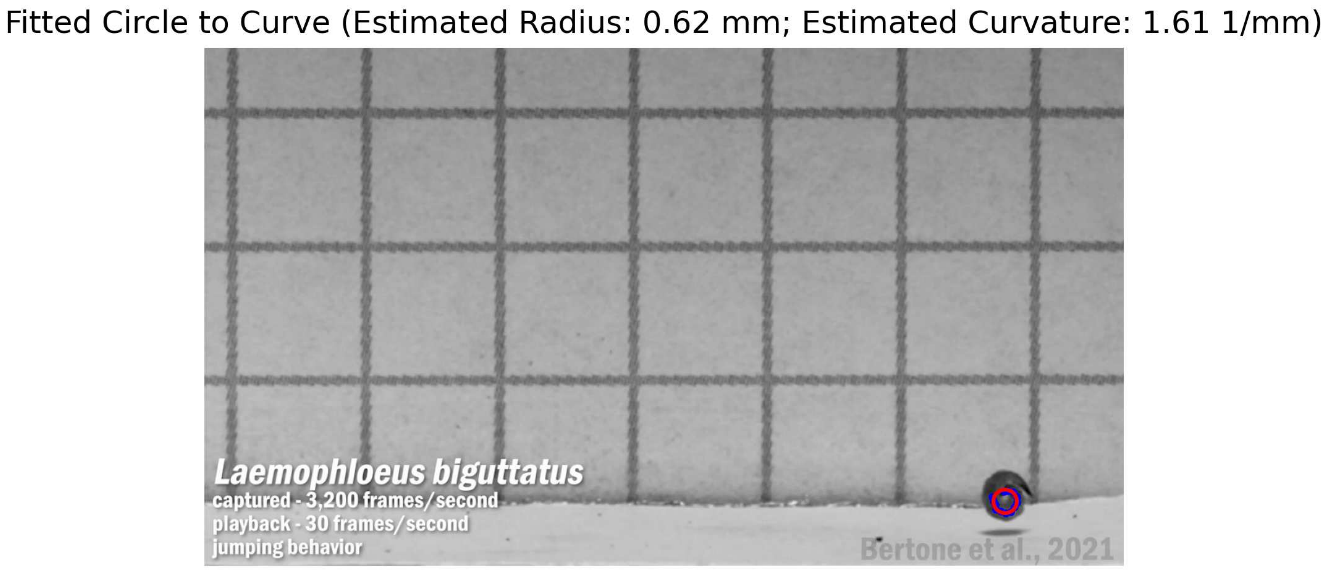

FIG. S5. Measurement of the radius of curvature for larval beetles by fitting a circle (in red). Adapted from Bertone *et al.* [7].

with

$$E_0^b(\ell,\kappa_0) = \int_0^{0.5}\left[\frac{1}{2}\,\Theta(S-S_0^L)\left(\frac{\mathrm{d}\theta_L^-}{\mathrm{d}S}-\ell\kappa_0\right)^2+\frac{1}{2}\,\Theta(-S+S_0^L)\left(\frac{\mathrm{d}\theta_L^+}{\mathrm{d}S}-\ell\kappa_0\right)^2\right]dS$$
$$+\int_{0.5}^{1}\left[\frac{1}{2}\,\Theta(S-S_0^R)\left(\frac{\mathrm{d}\theta_R^+}{\mathrm{d}S}-\ell\kappa_0\right)^2+\frac{1}{2}\,\Theta(-S+S_0^R)\left(\frac{\mathrm{d}\theta_R^-}{\mathrm{d}S}-\ell\kappa_0\right)^2\right]dS$$

(where $\Theta(x)$ is the Heaviside step function); and

$$Z_0^{L,\mathrm{nonlinear}}(S,\theta_0,S_0^L,\Lambda_Z^L,\ell,\kappa_0) \equiv \int_0^1 \mathrm{d}S\,\sin\theta$$
$$=\frac{1}{\ell|\kappa_0|\Lambda_Z^L}\Bigg[\sqrt{\Delta_L}\Big(\mathcal{E}\left(\tfrac{\pi-2\theta_0}{4},k_L\right)-\Theta(-S+S_0^L)\,\mathcal{E}\left(\tfrac{\pi-2\theta_L^+(S)}{4},k_L\right)$$
$$+\Theta(S-S_0^L)\left(\mathcal{E}\left(\tfrac{\pi-2\theta_L^+(S)}{4},k_L\right)-2\mathcal{E}\left(\tfrac{\pi-2\theta_L^+(S_0^L)}{4},k_L\right)\right)\Big)$$
$$-\frac{(\kappa_0\ell)^2+2\ell|\kappa_0|\Lambda_Z^L\sin(\theta_0)}{\sqrt{\Delta_L}}\Big(\mathcal{F}\left(\tfrac{\pi-2\theta_0}{4},k_L\right)-\Theta(-S+S_0^L)\,\mathcal{F}\left(\tfrac{\pi-2\theta_L^+(S)}{4},k_L\right)$$
$$+\Theta(S-S_0^L)\left(\mathcal{F}\left(\tfrac{\pi-2\theta_L^+(S)}{4},k_L\right)-2\mathcal{F}\left(\tfrac{\pi-2\theta_L^+(S_0^L)}{4},k_L\right)\right)\Big)\Bigg].$$

(All notations involved in these expressions are defined in §S2 A 2.)

E. Experiments with a curved strip

We observe in our experiments with a curved strip (see fig. 1c in the main text) a decay of the oscillations during the airborne phase after jumping. To estimate the damping H from these oscillations, we approximate the shape of the shell as a parabola, $z(x,t)=a_0\cos(\omega_0 t)\,x^2$, where a_0 is the amplitude of the parabola describing the shell at rest (fig. S1) and ω_0 is the natural frequency of the shell. Experimentally, we track three points on the shell: the two ends and the midpoint (see fig. S7). Assuming that the shell is perfectly symmetric, these three points create an isosceles triangle of base d_x and altitude d_z. With some trigonometry we then obtain an estimate of the oscillating amplitude

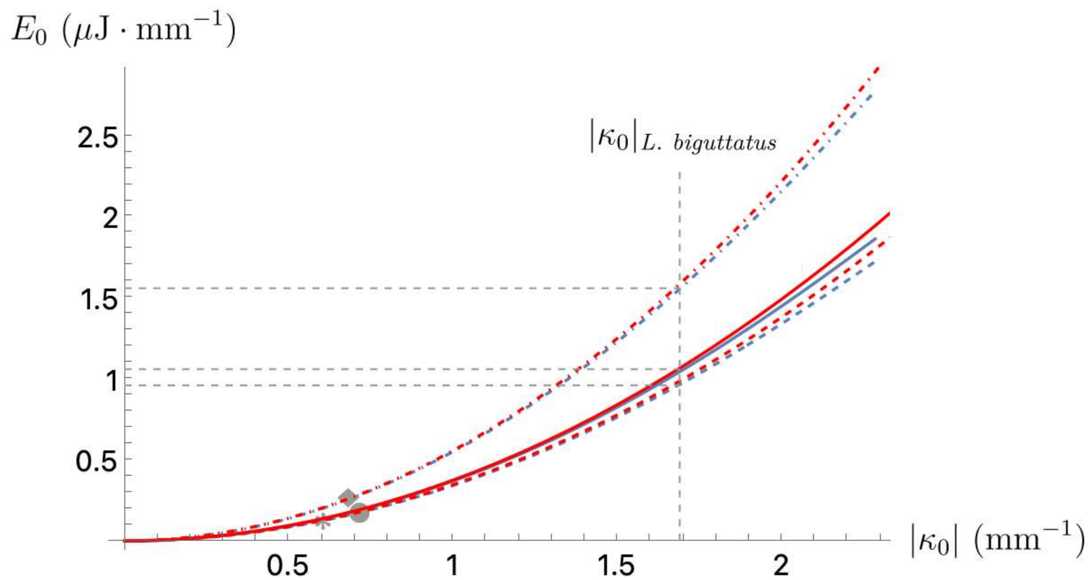

FIG. S6. Energy stored (gravitational+bending) of a latched cylindrical shell, with dimensions as per *Laemophloeus biguttatus* [7], as a function of the shell curvature (linearized theory in red and the non-linear model in blue). Gray symbols denote the stored energy per attachment point (or pair of legs for larvae) estimated by the corresponding curvature such that $F_0(\kappa_0) \sim \frac{1}{3}F_0[(\kappa_0)_{L.\ biguttatus}]$, and assuming the linear theory for $F_0(\kappa_0)$ (star for $E \sim 10$ kPa, circle for $E \sim 9.25$ kPa, and diamond for $E \sim 14.9$ kPa). Horizontal dashed lines show the stored energy at $|\kappa_0| = |\kappa_0|_{L.\ biguttatus}(= |\kappa_0^{\max}|)$ for the different cases.

of the shell

$$a(t) = \frac{d_z(t)}{d_x^2(t)}. \tag{S68}$$

We then fit the oscillations of $a(t)$ with $Z(X,T)$ from the linearized model in §S1. $Z(X,T)$ in this phase is described by the dynamic beam equation (S17) with free boundaries:

$$\left.\frac{\partial^2 Z}{\partial X^2}\right|_{X,0,1} = \frac{\kappa_0}{|\kappa_0|} \quad \text{and} \quad \left.\frac{\partial^3 Z}{\partial X^3}\right|_{X,0,1} = 0. \tag{S69}$$

We solve this boundary value problem (neglecting gravity, i.e. $\beta \gg 1$) by letting

$$Z(X,T) = \zeta(X,T) + w(X), \tag{S70}$$

where

$$w(X) = \frac{1}{2}\frac{\kappa_0}{|\kappa_0|}X^2, \tag{S71}$$

and $\zeta(X,T)$ is the separable solution

$$\begin{aligned}\zeta(X,T) = &\sum_{n=1}^{\infty} c_1^{(n)} \left[\left(\cos k_n X + \cosh k_n X\right) - \frac{\cos k_n + \cosh k_n}{\sin k_n - \sinh k_n}\left(\sin k_n X + \sinh k_n X\right)\right] \\ &e^{-\frac{H}{2}T}\left[a_n \cos\left(\omega_n T + \varphi_n\right)\right];\end{aligned} \tag{S72}$$

with

$$\omega_n = \frac{H}{2}\sqrt{\frac{4k_n^4}{H^2} - 1},$$

and k_n are the roots of the transcendental equation

$$\cos k \cosh k = 1. \tag{S73}$$

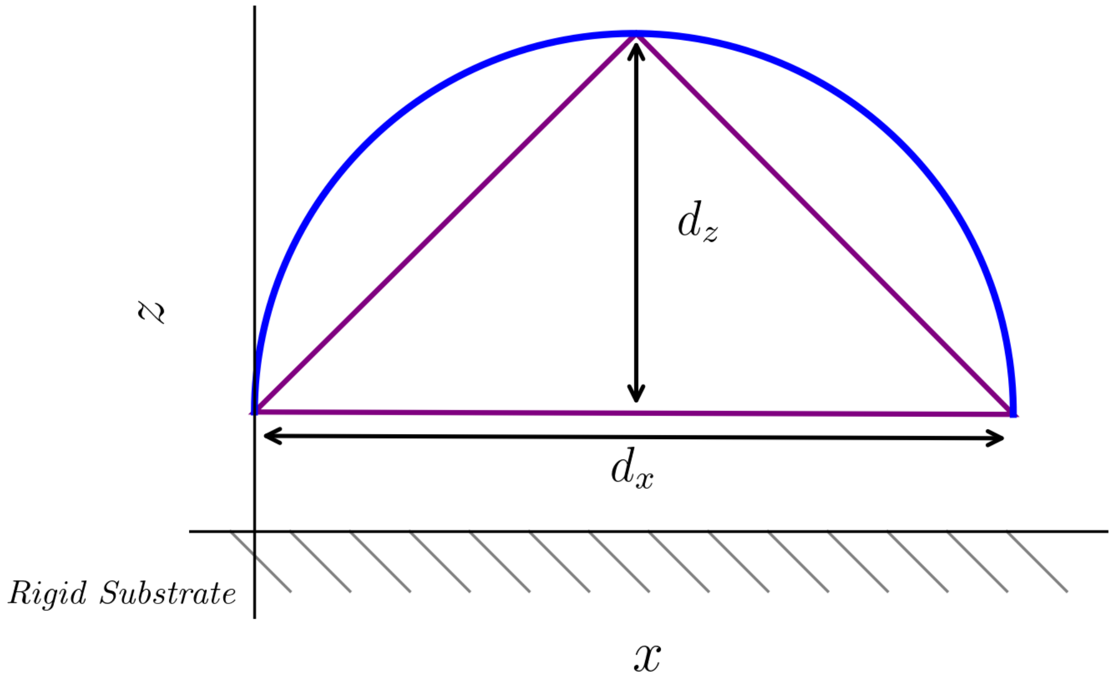

FIG. S7. Schematic representation of the cylindrical cap in the airborne phase, with a geometric model of the amplitude.

We fit the decay of the oscillations of $a(t)$ to the fundamental mode

$$\zeta_1(X,T) \propto e^{-\frac{H}{2}T}\left[\cos\left(\omega_1 T + \varphi_1\right)\right].$$

Note that we make the time T dimensional with the timescale $(\rho h \ell^4/EI)^{1/2}$, and have

$$\rho = 1.4 \cdot 10^3 \text{ kg} \cdot \text{m}^{-3},\, h = 0.3 \cdot 10^{-3} \text{ m}\,, \ell = 6.7 \cdot 10^{-3} \text{ m}\,, \text{ and } E = 2.3 \cdot 10^{-9} \text{ Pa}$$

in the experiments. The results shown in fig. S8 lead to the estimate of $H \sim 2$.

---

[1] B. Audoly and Y. Pomeau, *Elasticity and Geometry: From Hair Curls to the Non-linear Response of Shells* (OUP Oxford, 2010).
[2] R. G. Cox, The motion of long slender bodies in a viscous fluid part 1. general theory, J. Fluid Mech. **44**, 791–810 (1970).
[3] G. K. Batchelor, Slender-body theory for particles of arbitrary cross-section in Stokes flow, J. Fluid Mech. **44**, 419–440 (1970).
[4] P. Howell, G. Kozyreff, and J. Ockendon, *Applied Solid Mechanics*, Cambridge Texts in Applied Mathematics (Cambridge University Press, 2008).
[5] T. J. W. Wagner and D. Vella, The 'sticky elastica': delamination blisters beyond small deformations, Soft Matter **9**, 1025 (2013).
[6] T. A. Driscoll, N. Hale, and L. N. Trefethen, eds., *Chebfun Guide* (Pafnuty Publications, 2014).
[7] M. A. Bertone, J. C. Gibson, A. E. Seago, T. Yoshida, and A. A. Smith, A novel power-amplified jumping behavior in larval beetles (coleoptera: Laemophloeidae), PLOS One **17**, e0256509 (2022).
[8] A. C. Callan-Jones, P. T. Brun, and B. Audoly, Self-similar curling of a naturally curved elastica, Phys. Rev. Lett. **108**, 174302 (2012).

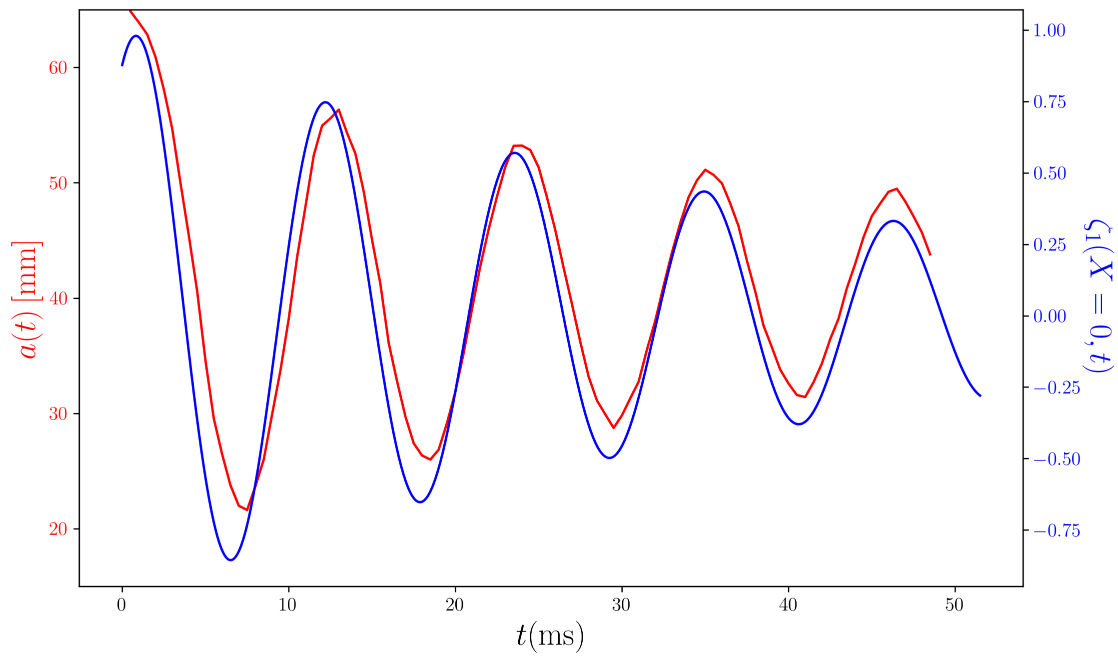

FIG. S8. Fitting the amplitude $a(t)$ in the experiments with the fundamental mode of the linearized theory.